Global carbon isotopic events in a Campanian–Maastrichtian deltaic succession (Tremp-Graus Basin, Spain) and multiproxy stratigraphy for high sedimentation rate environments

Constance Vinciguerra, Sophie Leleu, Delphine Desmares, Laurent Emmanuel, Luis Martinez, Corinne Loisy

Version of Record: https://www.sciencedirect.com/science/article/pii/S0195667122000866
Manuscript_db803114ad9248834fa795d1a96907b5

Global carbon isotopic events in a Campanian–Maastrichtian deltaic succession (Tremp-Graus Basin, Spain) and multiproxy stratigraphy for high sedimentation rate environments

Constance Vinciguerra [1*], Sophie Leleu [1], Delphine Desmares [2], Laurent Emmanuel[3], Luis Martinez[4], Corinne Loisy[1]

[1] EA 4592 Georessources et Environnement, ENSEGID-Bordeaux INP, avenue des Facultés, Talence 33400, France

[2] UMR 7207 CR2P, Sorbonne Université – MNHN - CNRS, 4, place Jussieu, 75005, Paris, France

[3] UMR 7193 ISTeP, Sorbonne Université - CNRS, 4, place Jussieu, 75005, Paris, France

[4]EOST, Université de Strasbourg, 1 rue Blessig, 67084 Strasbourg Cedex

[*]Corresponding author:sophie.leleu@bordeaux-inp.fr

Abstract

The Campanian to Maastrichtian sedimentary succession of the Tremp-Graus Basin (NE Spain) is characterized by the offshore-to-prodeltaic upper Vallcarga Fm giving way to prograding deltaic units (the Aren Fm), which are overlain by transitional facies (the Grey Unit) that correspond to the basal part of the Tremp Group. This work aims to improve the stratigraphical scheme of these deposits using a new dataset of $\delta^{13}C_{carb}$ and $\delta^{13}C_{org}$, $\delta^{18}O$ and TOC variations through time, supported by a new biostratigraphical analysis and compiling previous biostratigraphical and paleomagnetic data. The comparison of isotopic signals from marine reference sections where $\delta^{13}C_{carb}$ is well calibrated in the Tethys realm allows recognition of global isotopic events that can be used as correlative marker events. Significant high-frequency $\delta^{13}C$ variations defined in the $\delta^{13}C_{carb}$ are identified in the studied succession despite the different sedimentary setting and some can be related to global geochemical events such as the Late Campanian Event (LCE) and the Campanian–Maastrichtian Boundary Event (CMBE), in good agreement with the magnetic chrons at the base of the Tremp Group, and with some new biostratigraphic constraints. From multiple

geochemical and petrographic analysis of the organic matter we suggest that the geochemical signal corresponds to global changes, but at higher resolution, sedimentary dynamics are also reflected in the geochemical signals, particularly inputs of surface water in the deltaic signal.

Key words: $\delta^{13}C_{carb}$, $\delta^{13}C_{org}$, CMBE, LCE, Aren Sandstone

Introduction

When calibrated with biostratigraphy, stable carbon isotope profiles, both of carbonate ($\delta^{13}C_{carb}$) and organic matter ($\delta^{13}C_{org}$) samples, are a powerful tool for correlating and dating Cretaceous strata globally (Chenot et al., 2016; Gale et al., 1993; Jenkyns et al.,1994; Jarvis et al., 2002; Föllmi et al., 2006; Linnert et al., 2017; Voigt et al., 2012; Westerhold et al., 2011; Wendler, 2013). Chemostratigraphic studies based on carbon isotopes in bulk sediments are increasingly being used to achieve high-resolution correlations over large areas. However, complications arise from a multitude of possible influences due to local differences in biological, diagenetic and physicochemical factors on individual $\delta^{13}C$ signal that can mask the global signal (Wendler, 2013). Chemostratigraphic methods were developed and largely used in low energy carbonate marine rock records (e.g. Wendler, 2013 and reference therein), but more recently, many studies have been conducted on carbonate nodules in continental successions (Cojan et al., 2000; 2003; Lopez et al., 2000; Magioncalda et al., 2004; McInerney and Wing, 2011; Riera et al., 2013), on organic matter ($\delta^{13}C_{org}$) in marine successions (examples from Jurassic: Bodin et al., 2020; Upper Cretaceous: Jarvis et al,. 2006; Palaeocene: Storme, 2013), lagoonal successions with terrestrial input (Cretaceous, Heimhofer et al., 2003), andcontinental sedimentary successions (Maufrangeas et al., 2020; Yans et al., 2014). It has also been suggested by Heimhofer et al. (2003) that it is possible to correlate $\delta^{13}C$ records from deltaic organic matter with the $\delta^{13}C$ of marine reference successions. In most cases, $\delta^{13}C_{org}$ records show similar trends to the carbon isotopic signal from carbonate minerals ($\delta^{13}C_{carb}$) obtained from the

same material (Khozyem et al., 2013; Magioncalda et al., 2004; Storme, 2013; Tsikos et al., 2004). Differences in magnitude are due to vegetal tissues fractionating carbon in favor of ^{13}C. In marine sediments, $\delta^{13}C_{carb}$ is less negative (mean c. 0-1 ‰) than $\delta^{13}C_{org}$ (mean c. -23‰; Hayes et al., 1989; McInerney and Wing, 2011; Sharp, 2006). However the isotopic shifts can be slightly offset: in the PETM, for example, a delay of the $\delta^{13}C_{org}$ relative to the $\delta^{13}C_{carb}$ was documented by Khozyem et al. (2013). In some cases, the offsets between the two records coincide but showing opposing trends (e.g. Storme, 2013).

Although many high-resolution $\delta^{13}C_{carb}$ and $\delta^{13}C_{org}$ curves have been generated for Cretaceous marine and terrestrial successions (e.g. Heimhofer et al. 2003; Jarvis et al. 2006), and for the Palaeocene and the PETM (e.g. Aubry et al., 2007; Khozyem et al., 2013; Magioncalda et al., 2004; Röhl et al., 2007), only a few datasets, all based on $\delta^{13}C_{carb}$, exist for the Campanian–Maastrichtian stages (Chenot et al., 2016; Thibault et al., 2012; Voigt et al., 2010; 2012; Wendler, 2013).

The Tremp-Graus Basin (Fig.1) has been well-studied, but biostratigraphical analysis of its Upper Cretaceous successions failed to provide a high-resolution stratigraphical framework (Ardèvol et al., 2000; Caus and Gómez-Garrido, 1989; Díez-Canseco et al., 2014; Feist and Colombo Piñol, 1983; López-Martínez et al., 2001; Nagtegaal, 1972; Oms et al., 2016; Riera et al., 2009; 2010; Robles-Salcedo et al.,2013; Souquet, 1967; Vicens et al., 2004; Villalba-Breva and Martín-Closas, 2012). The scarce occurrences (due to environmental and depositional conditions) of poorly preserved planktonic foraminifera, coupled with the intermittent presence of environment-dependent markers such as benthic foraminifera and rudist bivalves, have not allowed precise constraints on the chronostratigraphic framework to be established for these Upper Cretaceous depositional sequences. As such, in our study we explored the use of continuous geochemical proxies as a stratigraphic tool.

Our aims were twofold: (1) to refine the stratigraphy of the Campanian to Maastrichtian in the south-eastern Pyrenean domain (Figs. 1, 2) during early orogeny, by establishing regional

and global correlations based on $\delta^{13}C_{carb}$; and (2) to test the response of $\delta^{13}C_{org}$ in order to compare both $\delta^{13}C$ signals and assess whether $\delta^{13}C_{org}$ could be used more widely. In this regard, after describing the sedimentary succession and its known stratigraphic markers, a new and continuous bulk $\delta^{13}C_{carb}$ and $\delta^{13}C_{org}$ dataset is presented, alongside measurements of $\delta^{18}O$, calcimetry and Total Organic Carbon (TOC). These analyses have been performed on 101 samples encompassing pro-deltaic, deltaic, and lagoonal deposits from the Orcau section of the northern Tremp-Graus Basin. We then present a correlation of our new $\delta^{13}C_{carb}$ dataset using the defined magnetostratigraphy of the Tremp-Graus Basin (Fondevilla et al., 2016), based on previous work (Canudo et al., 2016; Caus et al., 2016; Oms et al., 2007; Pereda-Suberbiola et al., 2009; Vicente et al., 2015; Villalba-Breva and Martin-Closàs, 2012) and some biostratigraphic markers found during this study, which give valuable anchor points for the geochemical dataset. The recognition of global geochemical events in the $\delta^{13}C_{carb}$ dataset reveals time constraints in this thick deltaic succession. Finally, we discuss the $\delta^{13}C_{org}$ signal relative to the $\delta^{13}C_{carb}$ trends and the signal provided by organic matter (OM) of various sources, which can be mixed in the sediments in various proportions, depending on the depositional environment.

1. Geological setting

1.1 Regional setting

The study area is located in the central part of the Southern Pyrenean Zone corresponding to a fold and thrust belt within the southern Pyrenean foreland basin that formed from the Late Cretaceous to the early Miocene (Deramond et al., 1993; Muñoz, 1992; Puigdefàbregas et al.,1992; Rosell et al., 2001; Teixell and Muñoz, 2000; Vergés et al., 2002; Fig. 1). The South-central Pyrenean Zone is divided into three sub-basins from north to south: the Organyà, the Tremp-Graus and the Àger Basins, which are East–West-trending basins defined by thrust-controlled sedimentation (Ardèvol et al., 2000; Vacherat et al., 2017). Our

study sections are localized in the Tremp-Graus Basin that is delimited by the Montsec thrust to the south, and the Bóixols thrust and associated Sant Corneli anticline to the north (Muñoz, 1992; Puigdefàbregas et al., 1992; Teixell and Muñoz, 2000; Vergés et al., 2002), the latter generated by the inversion of pre-existing E-W faults during Santonian.

1.2 Sedimentology and stratigraphy in the Tremp-Graus Basin

The Tremp-Graus Basin sedimentary successions related to the foreland basin development during the uppermost Cretaceous to Palaeocene times are composed of (1) Santonian to Campanian slope and prodelta deposits, i.e. the Salàs marls, upper part of the Vallcarga Formation, (2) Campano-Maastrichtian shoreface deposits, i.e. the Aren Formation, (3) Maastrichtian lagoonal facies, i.e the Grey Unit of the Tremp Group, and (4) Maastrichtian to Thanetian continental red beds (Garumnian facies), i.e. the main Tremp Group (Fig. 2).

The Salàs marls correspond to a very thick unit of about 1500 meters that consist of grey marls giving way to sandy beds at the top of the succession. The sandstones are turbiditic erosive beds of a few centimeters in thickness (Ardèvol et al., 2000; Mey et al., 1968; Nagtegaal, 1972; Souquet, 1967). Turbiditic deposits consist of erosive fining-upwards lenses of fine-grained sandstones that commonly display well-developed Bouma sequences (Mey et al., 1968; Nagtegaal, 1972; Puigdefàbregas and Souquet, 1986; Souquet, 1967;). The Salàs marls contain abundant mudstone clasts and foraminifera, and occasionally cohesive debris flows and slump structures (Souquet, 1967; Souquet and Deramond, 1989). The unit is attributed to the successive Santonian and Campanian planktonic foraminifera biozones *Dicarinella asymetrica*, *Globotruncanita elevata*, *Globotruncana ventricosa* and *R. calcarata* (Ardèvol et al., 2000) but no detailed study of the biostratigraphic content is published.

The Salàs marls grade transitionally into the Aren Fm, which becomes sandier towards the top, with thicker and more amalgamated sandstone beds (Mey et al., 1968). The Aren Fm contains quarzitic grains with bioclasts, echinoderms, rudists, bryozoans and foraminifera

(Souquet, 1967; Riera et al., 2009). The Lower Aren Unit shows grey clayish and silty marl with intercalations of calcarenite and limestone beds forming small coarsening-up sequences (Nagtegaal, 1972 - Fig. 2).

The Upper Aren Unit is typically made of erosive beds and medium- and larger-scale cross-bedding sets (Nagtegaal et al., 1983) that indicate a highly hydrodynamic deltaic system (Mutti and Sgavetti, 1987; Nagtegaal et al., 1983). These cross-bedded sandstones are very-coarse to medium-grained and well-sorted, forming beds from 10 centimeters to several meters in thickness, from which paleocurrent measurements indicate unidirectional westward flows. The Upper Aren Unit shows four progradant deltaic sequences (CuS1 to CuS4) formed of coarse-grained sandstones, alternating with marl deposits at the base of each coarsening-up sequence (Fig. 2). It contains particularly abundant bioclasts, echinoderms, rudist debris, bryozoans, foraminifera, burrows, suggesting a nutrient-rich depositional environment favouring a diverse benthic fauna (Souquet, 1967; Mey et al., 1968; Nagtegaal,1972; Nagtegaal et al.,1983; Ardèvol et al., 2000; Robles-Salcedo et al., 2013). Some rudists in life position are intercalated in the upper part of the deltaic deposits, indicating rudist patches (Díaz-Molina, 1987; Nagtegaal, 1972; Nagtegaal et al.,1983) developing in more sheltered areas on the shelf (Vicens et al., 2004). The top of the Upper Aren Unit shows a very distinct facies with abundant large-scale hummocky cross-stratification (HCS) which indicates a wave-dominated delta environment (Nagtegaal et al., 1983). This deltaic system flowing westwards is associated with an important and rapid thickness increase of the Aren Fm westwards in the Tremp-Graus Basin, attesting to syn-depositional movement of the Bóixols thrust (Ardèvol et al., 2000). In recent years, the stratigraphic division of the Aren Fm has changed. Indeed, previous authors (Souquet, 1967) attribute all the Aren Fm to the upper Maastrichtian, while recent studies (Robles-Salcedo et al., 2013) attribute the Lower Aren Unit to the Campanian and the Upper Aren Unit to the Maastrichtian based on the *Globotruncana falsostuarti* planktonic foraminifera zone and the *Pachydiscus neubergicus* ammonite zone. However, the boundary between the Campanian

158 and the Maastrichtian is still very poorly defined and could be placed within tens of meters in
159 the sedimentary succession.

160 The Aren Fm is overlain by the Tremp Group which is subdivided into different formations
161 (Cuevas et al.,1989; López-Martínez et al., 2006; Pujalte and Schmitz, 2005; Riera et al.,
162 2009; Rosell et al., 2001) : the Grey Unit, or La Posa Formation, forms its base, overlain by
163 the first Red Bed unit: the Conques Formation. It consists of lagoonal and shallow marine
164 deposits (Cuevas, 1992; Nagtegaal et al., 1983; Riera et al., 2009; Rosell et al., 2001).
165 Lagoonal deposits are composed of greyish marls which contain ostracods, charophytes,
166 plant remains, fragments of bivalves and benthic foraminifera (Díez-Canseco et al., 2014;
167 Riera et al., 2009; Robles-Salcedo et al., 2018; Rosell et al., 2001), and sandy limestones
168 with accumulations of *Corbicula* (Bivalvia), *Lychnus* and *Cerithium* (Gastropoda), ostracods,
169 benthic and planktonic foraminifera, dasycladacean algae and charophytes (Díez-Canseco et
170 al., 2014). Locally abundant dinosaur footprints and pedogenic structures suggest that the
171 area was close to the lagoon margin with very low water depth, with occasional emergent
172 phases (Díez-Canseco et al., 2014). These lagoonal and nearshore facies are interbedded
173 locally with a lens of very coarse-grained yellow sandstones, overlain by rudists (*Hippurites*
174 *radiosus*) in life position. The presence of rudists indicates a marine incursion in the lagoon
175 and the development of a shallow and sheltered marine environment (Vicens et al., 2004).
176 The Grey Unit corresponds to the transition from a shoreface environment (Aren Fm) to a
177 terrestrial domain: the Garumnian facies, which directly overlies the Grey Unit (Nagtegaal et
178 al.,1983; Cuevas, 1992; Rosell et al.,2001; Riera et al., 2009).

179 The *Hippurites radiosus* beds in the uppermost Aren Fm were regarded as isochronous by
180 previous authors and attributed to the early Maastrichtian age (Caus et al., 2016; Oms et al.,
181 2007; Díez-Canseco et al., 2014; Vicens et al., 2004; Vicente et al., 2015). Additionally
182 charophytes found in basal beds of the Grey Unit to the east of the Tremp-Graus Basin
183 (Villalba-Breva and Martin-Closàs, 2012) as well as further east (Vicente et al., 2015). These,
184 together with associated paleomagnetic data, suggest the basal beds of the Grey Unit belong

to Chron 32 (Oms et al., 2007, 2016), while most of the Grey Unit is recorded as Chron 31r (Fondevilla et al., 2016; Fig. 2). Using the Geomagnetic Polarity Time Scale of Ogg and Hinnov (2012), Fondevilla et al (2016) located the C32/ C31r at the base of the Grey Unit.

2. Methods

2.1 Field work and sampling

The 320 m-thick succession at Orcau preserves the evolution from marine to deltaic to lagoonal environments. It was logged in detail to determine sedimentary facies and allocate stratigraphic units as well as to compare the magnetostratigraphic and biostratigraphic records (Fig. 2) of previous authors. One hundred and one samples were collected for geochemical analysis (Figs. 2, 3) with average spacing between samples of 1.95 m; these were collected in a manner that ensured no present-day organic matter (e.g. roots or oxidation traces) could contaminate the isotopic analysis. Some intervals could not be sampled due to vegetation cover (between 118 and 135.9 m in the section). Only 83 samples underwent the complete multiproxy isotopic study ($\delta^{13}C_{carb}$, $\delta^{13}C_{org}$, $\delta^{18}O$ and TOC; Fig. 3). Some samples were specifically taken for organic matter characterization (6 samples) and biostratigraphic analysis (23 samples; Fig. 2).

2.2 Microfossils

Following standard procedures, marlstones were soaked overnight in a dilute solution of hydrogen peroxide and subsequently washed over 63 μm and 1 mm sieves. The microfossils were extracted from the 63 μm–1mm fraction. Due to their poor state of preservation, most of the specimens were observed by scanning electron microscopy (SEM) analysis. For the sandstone beds, foraminifera and other bioclasts have been identified in thin section. 14 residues and 15 thin sections have been studied (Figs. 2, 4, 5, 6).

2.3 Carbonate content and TOC

Calcium carbonate contents ($CaCO_3$ in weight percent) were measured at Sorbonne Université (Paris, France) on 90 samples (Figs. 2, 3) using the carbonate bomb technique, which measures the CO_2 pressure created by 30% HCI dissolution of 100 mg of dried bulk carbonate sample in a sealed reaction cell. The resulting pressure increase is then measured with a manometer and compared to a calibration curve previously obtained by measurements of reagent-grade $CaCO_3$ (Carlo Erba). The precision of the used carbonate bomb is less than 1% for $CaCO_3$ values >10%. The absolute accuracy is 1% for $CaCO_3$ values >10%.

The TOC analyses were performed on-line using the Thermo Scientific EA IsoLink IRMS System at CRPG laboratory (Nancy, France) on 91 decarbonated samples (Figs. 2, 3). In order to have total rock values it was necessary to make the following correction:

$$TOC\ total\ rock\ = TOC\ decarb * (100 - calcimetry\ value)/100$$

2.4 Bulk carbonate stable isotopes ($\delta^{13}C_{carb}$, $\delta^{13}C_{org}$, $\delta^{18}O$)

Stable isotope analyses ($\delta^{13}C_{carb}$ and $\delta^{18}O$) were performed on 90 bulk carbonate samples at Sorbonne Université (Paris, France) using a Kiel IV carbonate device and a DELTA V Advantage isotope ratio mass spectrometer. Oxygen and carbon stable isotope values were obtained by analyzing carbon dioxide generated by the dissolution of bulk carbonate samples using anhydric orthophosphoric acid at 70°C. Isotope values (Fig. 3) are reported in delta (δ) notation, relative to Vienna Pee Dee Belemnite. Accuracy and precision of 0.03‰ and 0.08‰ (1 σ) for carbon and oxygen respectively were determined by repeated analyses of a marble working standard, calibrated against the international standard NBS-19.

The measurements of the $\delta^{13}C_{org}$ were performed on-line using the Thermo Scientific EA IsoLink IRMS System at CRPG laboratory (Nancy, France). Before $\delta^{13}C_{org}$ isotopic measurements, 91 samples were prepared following a protocol described by Magioncalda et

al. (2004) and Storme (2013). The bulk samples were cleaned, dried and grinded, and the sample powders were treated with 25% HCl solution for decarbonatation. Sample acidity was then neutralized by multiple centrifugations with pure water, and finally residues were dried at 30° Celsius and powdered again. Decarbonated samples were wrapped in tin capsules and loaded in a specific auto-sampler connected to the EA and pumped out for 20 minutes before opening it to the combustion reactor at 1020°C. Produced gases (N_2, CO_2) were separated on a chromatographic column and the carbon isotopic composition of the produced CO_2 was measured with a Thermo Scientific Delta V Advantage isotope ratio mass spectrometer. Both carbon concentration and isotopic composition were determined twice per sample by comparison with two internal and two international standards routinely included during the analysis: (1) BFSd (C = 0.53 wt.%; $\delta^{13}C$ = -21.5‰), (2) CRPG_M2 (C = 0.408 wt.%; $\delta^{13}C$ = -24.98‰), (3) PSd (C = 0.03 wt.%; $\delta^{13}C$ = -22.4‰) and (4) JG-3 Granodiorite powder (C = 0.012 wt.%). Values are quoted in the delta notation in ‰ relative to V-PDB (Fig. 3), and the analytical precision is within 0.3 ‰ (1σ).

2.5 Organic matter (OM) petrographical analysis

To define the source of organic matter, petrographical analysis was performed on a set of 6 samples from throughout the stratigraphic column (Figs. 2, 7, 8). These samples were taken from the Orcau section, five from the Aren Fm and one from the Grey Unit. The maceral analyses were carried out on a piece of rock impregnated with epoxy resin to carry out the optical observations in a LEITZ MPV3 microscope. The microscope equipped to observe the OM in natural light (reflected and transmitted) and fluorescence (same objective) shows a maximum resolution of 1 micron. With the 50X objective that we use for observations we can work in oil immersion and take advantage of a better light transmission and reflection.

256 **3. Results**

257 **3.1 Sedimentary sequences and stratigraphic attributions**

258 The 325 m-thick Orcau section displays facies of bioturbated bluish marls interbedded with
259 laminated and cross-bedded sandstones at its base attributed to the Lower Aren Unit and
260 interpreted as offshore prodelta deposits (Nagtegaal, 1972; Robles-Salcedo et al., 2013;
261 Figs.2, 3).

262 A thicker marly-rich interval between 120 and 180 m corresponds to the uppermost Lower
263 Aren Unit well defined by Nagtegaal (1972) and below the coarser and sandier units
264 containing abundant bioclastic debris that defines the coarse calcarenite facies of the Upper
265 Aren Unit (Fig. 2). Within the Lower Aren Unit, the sedimentary section shows intervals
266 containing very few, thin sandstone beds, while other intervals show thicker and more
267 abundant sandstone beds forming high frequency sedimentary sequences (Fig. 3).

268 The Upper Aren Unit shows four coarsening-up progradational sequences (CuS1 to CuS4),
269 each starting with marly intervals and ending with erosive, very coarse-grained sandstones
270 (between 180 and 295 m) corresponding to the Aren Fm *sensustricto* (Fig. 3; Nagtegaal,
271 1972; Nagtegaal et al.,1983; Ardèvol et al., 2000). The last coarser unit displays well-
272 developed large hummocky cross-stratification (288 to 296 m, Fig. 2) and marks the end of
273 the Aren Fm as described by Nagtegaal (1972); Nagtegaal et al. (1983) and Hoyt (1967).
274 The age of the Aren Fm was defined to late Campanian-early Maastrichtian and recently
275 (Robles-Salcedo et al., 2013) the position of the Campanian–Maastrichtian boundary was
276 placed between the Lower and the Upper Aren Unit (at 175 m, Fig. 2). Due to the lack of bio-
277 markers and their poor preservation, the chronostratigraphic scheme of this formation is still
278 poorly defined.

279 The sedimentary succession between 295 and 325 m (Fig. 2) is attributed to the Grey Unit,
280 based on very contrasting facies compared to the underlying Aren Fm. It starts with
281 carbonate beds interbedded with grey marl deposits, containing burrows, bioclasts, debris of

benthic foraminifera, bivalves, charophytes and plant remains (Fig. 2), well-described in previous publications (Cuevas, 1992; Nagtegaal et al., 1983; Riera et al., 2009; Rosell et al., 2001). It also contains spectacular beds with the presence of dinosaur tracks that indicates a more coastal and quieter environment, like a lagoonal or lacustrine area (Díez-Canseco et al., 2014; Robles-Salcedo et al.,2018; 297 m, Fig. 2). The top of the Grey Unit in the studied section is marked by a large lens of yellow coarse-grained sandstone (shoreface sandstone) overlain by rudists in life position forming small patches (Robles-Salcedo et al., 2018; at 315 m on Fig. 2), and a final lens of large oncoid conglomerates within the dark clays (320.8 m, Fig. 2). The section ends with the onset of the Conques Fm, which is dominated by red and mottled claystones, intercalated upwards with large lenses of fluvial sandstones. The attribution of magnetic chrons by Fondevilla et al. (2016) is possible based on sedimentary facies and biostratigraphical comparisons (Oms et al., 2007, 2016; Vicens et al. 2004; Vincente et al., 2015). Fondevilla et al. (2016) attributed the base of the Grey Unit to the top of Chron32n and the overlying Grey Unit facies to the Chron31r. So the boundary C32/C31r is defined at 299 m in our Orcau log section, in the first sandstone bed just above the base of the Grey Unit (Fig. 2). However, the lower boundary of Chron32 was not targeted and thus not located. No magnetostratigraphic study was carried out beneath the top of the Chron32, however the overlying entire Conques Fm belongs to Chron31r (Fondevilla et al., 2016).

3.2 Biostratigraphy studies

Ten of the 14 washed sediments from the Lower Aren Unit and from the base of the Upper Aren Unit have yielded planktonic foraminifera (Figs. 2, 4). However, they are rare and in a poor state of preservation. They show several taphonomic alterations including test fragmentation, abrasion, recrystallization and chamber fillings (Fig. 4). The species richness is low for such Upper Cretaceous deposits; nineteen species have been determined. Despite the detrital nature of the Aren Fm no sign of reworking has been observed. Though it has yielded insufficient index species to establish a formal zonal scheme, the planktonic foraminiferal succession is consistent (middle/upper Campanian to lower Maastrichtian) and

does not present any reworked specimens (i.e. with last occurrence older than middle Campanian). Among keeled forms, *Globotruncana* are the most common and are mainly represented by species with a long stratigraphical range (first occurrences within the Santonian Stage – last occurrences within the Maastrichtian Stage): *Globotruncana arca*, *Globotruncana hilli*, *Globotruncana lapparenti*, *Globotruncana lineianna, Globotruncana mariei*, *Globotruncana neotricarinata* (Figs. 2, 4). In sample OR-02-17, *Globotruncana aegyptiaca* (Figs. 2, 4) has been identified, indicating that this upper part of the Lower Aren Unit is at least late Campanian in age. It is in agreement with the presence of *Rugotruncana subcircumnodifer*, which first occurs in the late Campanian. At the base of the Upper Aren Unit, in samples OR-02-19 and OR-02-20, *Globigerinelloides messinae* has been identified (Figs. 2, 4). In sample OR-02-20, *Globotruncanella pschadae* has been found. First occurrences of these two species are usually recorded in the *Gansserina gansseri* zone (Petrizzo, 2001; Arz and Molina, 2002; Mesozoic planktonic foraminifera "PF@Mikrotax" available at http://www.mikrotax.org/pforams/index) that spans the Campanian–Maastrichtian boundary. It is in agreement with the occurrence of *G. gansseri* within the sample 0R-02-20. The last observed planktonic foraminifera of our sampling have been found in this sample (Fig.2). The next biostratigraphic markers in the stratigraphy have been provided by large benthic foraminifera observed in thin sections (Figs. 2, 5, 6) from highly indurated sandstone beds. Species of the genera *Siderolites* are a good biostratigraphic marker to constrain the position of the Campanian–Maastrichtian boundary in shallow marine facies (Robles-Salcedo, 2014; Robles-Salcedo et al., 2018). Among them, *Siderolites* with well-developed spines only occur in the Maastrichtian. Samples OR-02-21 and OR-03-314 present *Siderolites* with well-developed spines (Figs. 2, 5, 6) indicating that these levels are Maastrichtian in age. Thus, the Campanian–Maastrichtian boundary should be placed in the lower part of the Upper Aren Unit. This is in accordance with previous biostratigraphic works. Villalba-Breva and Martín-Closas (2012) assigned the charophytes-rich beds of the subsequent Grey Unit in the eastern part of the Tremp–Graus Basin to the lower Maastrichtian. Díez-Canseco et al. (2014) have interpreted in situ (non-reworked) planktonic

337 foraminifera assemblages of the Grey Unit and the Lower Red Unit of the Tremp Group as
338 lower to upper Maastrichtian.

339 ### 3.3 TOC and $CaCO_3$ values

340 The stratigraphic variations in TOC and %$CaCO_3$ from the Orcau section are shown in Figure
341 6 and provided in Supplementary Table 1.

342 The TOC values at Orcau range from 0.02% to 4.36% with a mean of 0.53%. The Lower
343 Aren Unit at the base of the section (0-113.5 m) is characterized by a constant TOC with an
344 average value of 0.33%. The end of the Lower Aren Unit and the beginning of the Upper
345 Aren Unit (113.5-211.9 m) is characterized by increasing TOC with an average value of
346 0.73%. The remainder of the Upper Aren Unit (211.9-295 m) shows a TOC value of 0.20%.
347 The Grey Unit at the top of the section (295-320.8 m) is characterized by an increasing TOC
348 with an average value of 1.90%. The richest samples in organic matter are from lagoonal
349 carbonates of the Grey Unit (Fig. 3).

350 The carbonate contents range from 23% to 99% with a mean at 73%. Most calcimetric
351 values vary between 60% and 85% while 2 samples exhibit significantly low values of 45%
352 and 39% (Fig. 3) in the Lower Aren Unit, corresponding to sandstone lithologies. A sample
353 from the Grey Unit exhibits the lowest value (23%). Two samples in the Grey Unit that are
354 carbonate mudstone show, not surprisingly, a proportion of $CaCO_3$ at 99% and 97% while
355 four samples of calcarenite lower in the section also show a high $CaCO_3$ proportion.

356 ### 3.4 Stable isotopes ($\delta^{13}C$, $\delta^{18}O$)

357 Several positive and negative shifts and excursions are evident, as well as long-term trends
358 well exhibited in Figure 3 both in the $\delta^{13}C_{carb}$ and the $\delta^{13}C_{org}$ values.

359 The $\delta^{13}C_{carb}$ of the Orcau dataset displays values ranging from -6.63‰ and +1.45‰ (vs
360 VPDB) that are relatively low values. At the base, the $\delta^{13}C_{carb}$ data show an irregular signal
361 followed by a positive shift between 47 and 70 m (Fig. 3). A well-marked negative excursion

occurs between ~72 m and 89 m. The upper transition of this negative excursion is sharp. More regular and more constant positive values between +1.02‰ and +1.44‰ depict a thick succession up to 162 m that is followed by a long-term trend to increasingly negative values. This general trend is arranged into successive and progressive decreases (162-212 m; 212-255 m; 255-282 m; 282-297 m) with the last sequence appearing in the Grey Unit, starting with a sharp negative shift and showing an amplitude higher than 3‰ at the top (297-320 m; Fig. 3).

The $\delta^{13}C_{org}$ values from the Orcau dataset range from -27.1‰ to -21.7‰. The main negative excursions correspond to an amplitude higher than 2‰ (47.4 to 65.6 m and 290 to 305 m; Fig. 3), with the maximum amplitude of -2.9‰ at 295 m. At the base, the $\delta^{13}C_{org}$ data show a small positive trend, followed by negative trend from 38 to 70 m. A positive excursion is recorded from 70 to 89 m, and followed by values around -25‰ up to 162m. Several positive trends are observed (162-205 m; 205-225 m; 225-255 m) followed by a negative trend at the top of the Upper Aren Unit (255-298 m). A sharp excursion marks the transition to the Grey Unit: the most negative value is recorded at the base of the Grey Unit in a sandstone bed and followed by the maximum amplitude (1.9‰) of a positive excursion at 311.5 m.

The $\delta^{18}O$ values vary between -8.07‰ and -1.79‰ (vs VPDB). They generally present "normal" values for marine environments in the Aren Fm but do show a global trend towards lower values from the base of the section to the top of the Aren Fm. In general, the values of the stable isotopes of carbon and oxygen show a covariant evolution from the base of the outcrop to the upper part of the Upper Aren Unit. In the terminal part of the Upper Aren Unit and in the Grey Unit, the isotopic records of carbon and oxygen show trends that are in opposition (Fig. 3).

3.5 Organic matter

The six samples contained sufficient large clasts of organic matter to be optically observed: OR-40.8 and OR-158 were collected from sandstones of the Lower Aren Unit; OR-191 and

OR-248.5 were collected from sandstones of the Upper Aren Unit; and OR-305.3 and OR-311.5 m were collected from a carbonate bed of the Grey Unit.

They yield organic matter from both continental and marine origins (Figs. 7 and 8). Two samples in particular (OR03-191 and OR03-158; Figs. 7 and 8) contain non-fluorescent organic matter of continental origin (Fig. 7 A, B, C, D, E, F, G, H) that can be clearly observed with particles of size that range from 5 to >250 µm (Fig. 7 C, G). The amorphous marine kerogen is often fluorescent (Fig. 7 B; Fig. 8 E, F, G) with a color tone located at 460 nm and of immature OM (excitation in fluorescence with a 365 nm mercury lamp). RO % (vitrinite reflectance), vitrinite and telinite particles confirms this result with a % RO of less than 0.5% (Fig. 7 E, F, G, H).

Most samples have low OM content as % TOC is low, as confirmed by Rock-Eval pyrolysis results. Consequently, the interpretation of the pyrolysis analysis (the ratio of the S2 / S3 peaks of origin) is very difficult because, as the petrographic analysis shows, the measurements are reliable only in two-thirds of samples. However, in the two samples showing continental organic matter (Fig. 7 and 8, with inertinite and pyrite), it can be said that river transportation with erosion can be observed in the rounding of physically degraded and sometimes chemically oxidized vitrinite particles (Fig. 7 A and Fig. 8 D).

4. Discussion

We have found no correlation between isotopic values: Figure 9 suggests no post-depositional bias and particularly no burial diagenesis impacting on the geochemical signal (Oehlert and Swart, 2014) for the Lower and Upper Aren Units. However, due to a small number of values in the Grey Unit and particularly low values of the $\delta^{13}C_{carb}$ associated with OM-rich beds, some burial effect may be suspected (Bodin et al., 2016; Wohlwend et al., 2016) and will be discussed below.

4.1 High-resolution stratigraphy in deltaic successions

Many stable bulk isotope studies are available for Campano-Maastrichtian successions in fully marine sections (Jarvis et al., 2002; Jung et al., 2012; Linnert et al., 2017; Paul and Lamolda, 2007; Thibault et al., 2012; Voigt et al., 2010; 2012; Wendler, 2013), and have been used to define several isotopic events and long-term trends as global stratigraphic markers, such as the MCE - Mid-Campanian Event (positive excursion), the LCE - Late Campanian Event (negative excursion), the CMBE - Campanian–Maastrichtian Boundary Event (negative excursion), and the MME - Mid-Maastrichtian Event (a two-stepwise positive excursion). Some of these are brief and more or less pronounced negative and positive Carbon Isotopic Excursions (CIE) and correspond to environmental changes.

The $\delta^{13}C_{carb}$ variations in the studied Orcau sedimentary succession allows the definition of high-resolution temporal sequences (Figs. 3, 10), corresponding to trends and excursions in the $\delta^{13}C_{carb}$ dataset. Subsequently, we propose a correlation between the $\delta^{13}C_{carb}$ record of the Tremp-Graus Basin and the $\delta^{13}C_{carb}$ records of two marine Campanian to Maastrichtian reference sections (Fig. 10), at Tercis-les-Bains (Voigt et al., 2012) and Gubbio (Coccioni et al., 2012) that correspond to different sedimentary depositional environments. The Gubbio sedimentary facies are pelagic sediments while the Tercis-les-Bains succession shows an alternating marl and limestone succession of a carbonate slope. Therefore, differences in sedimentary environments and sedimentation rates for each section must be taken into account in order to be able to achieve large-scale spatio-temporal correlations.

At Orcau, the boundary between the Campanian and Maastrichtian is not precisely known because biostratigraphical markers (planktic or benthic foraminifera) are not able to provide continuous high-resolution stratigraphical framework. This is due to their scarcity and their poor preservation in the Upper Cretaceous pro-delta system of the Tremp-Graus Basin (Ardèvol et al., 2000; Feist and Colombo Piñol, 1983; López-Martínez, 2001; Oms et al., 2016; Riera et al., 2009; 2010 and references therein; Vicens et al., 2004; Villalba-Breva and Martín-Closas, 2012). As such, our use of continuous geochemical multiproxies as a tool for

stratigraphy is appropriate. However, the occurence of *Siderolites* with well-developed spines (sample OR-02-21) confirms that this bed (at 198 m) is Maastrichtian in age.

The characteristic isotopic events of the CMBE, in agreement with the magnetostratigraphic and biostratigraphic data, could allow us to define the Campanian–Maastrichtian boundary in the dataset. The CMBE is defined by a succession of several negative and positive trends on either side of the Campanian–Maastrichtian boundary, and lies across the Chron32n and 31r such as identified on the $\delta^{13}C_{carb}$ curve from Gubbio, and partly identified in the Tercis-les-Bains section (Voigt et al., 2012). The base of the CMBE is marked by a positive excursion followed by a negative trend below the Campanian–Maastrichtian boundary in the Chron32n. This isotopic event is identified in the Orcau isotopic curve at 163.2 m (A1 on Fig.10) but it is relatively narrow because it corresponds to a sedimentary highstand unit (marly offshore delta), and we lack samples from this interval. It is followed by a subtle switch in the values in Tercis-les-Bains, and with a negative trend in Gubbio (A2 in Fig. 10), up to relatively negative values (around - 1‰ (vs VPDB). A well-expressed positive shift marks the middle part (A3) of the CMBE located on the Chron32/C31 boundary in Gubbio. It corresponds to the upper part of the Orcau section, suggesting a high sedimentary accumulation in Orcau despite an enclosed lagoonal environment with minor sedimentary fluxes.

Below the CMBE, the Late Campanian Event (LCE) might be expected in the Orcau section. It is defined by a prominent negative excursion at the end of the Chron33n and in the *R. calcarata* Zone, and is particularly well expressed in Tercis-les-Bains (Coccioni et al., 2012; Jarvis et al., 2002; Li et al., 2006; Thibault et al., 2012; Voigt et al., 2012). A significant negative excursion is seen between 70 and 89 m (noted B) with isotopic values around 0.00 ‰ framed by two more negative values (- 3.31‰ at 76.2 m and - 4.81‰ at 87.00 m). We suspect that the LCE would fall within this B interval. Another negative excursion starting from the base of the section between 23 and 59 m (noted C), with isotopic values around 0.5 ‰ but only one very negative value at – 2.90‰ (48.50 m), could correspond to the excursion

beneath the LCE that is seen clearly in the Tercis-les-Bains dataset. It may be expanded in Orcau section due to a higher sedimentary accumulation rate.

Between the LCE and the CMBE, similar trends are observed on the reference curves as well as on the Orcau isotopic curve between 88 and 162 m, with a constant trend showing values around + 1.10‰.

4.2 Depositional environment and its influence on the $\delta^{13}C$ record?

Previous works show that all isotopic carbon signals are influenced by several factors, the most important of which is the atmospheric carbon dioxide and pCO_2 (Arens et al., 2000; Wendler, 2013). Marine $\delta^{13}C_{carb}$ is generally more positive than terrestrial $\delta^{13}C_{carb}$ due to the interaction with meteoric water (Sharp, 2006). The $\delta^{13}C_{carb}$ in marine carbonates is either in equilibrium with the isotopic composition of the ocean water at the time ($\delta^{13}C_{carb}$ around 1‰) or reflects the vital effect of the various organisms that form carbonate rocks (between - 12 to + 1‰), while the $\delta^{13}C$ of bulk organic matter in marine deposits is influenced by oceanic productivity and terrestrial inputs (Hilting et al., 2008). The measurement of organic carbon isotope composition in sediments is most similar to the average composite sample of many species, which minimizes the physiological bias of the life effect (Arens et al., 2000; Jahren et al., 2001). Amongst deltaic Upper Cretaceous deposits organic matter could come from terrestrial C3 plants, peat and coal/lignite from land, bearing $\delta^{13}C_{org}$ mean values between – 33 to – 23‰ (Cerling and Quade, 1993), or from aquatic photic organisms with $\delta^{13}C_{org}$ ranging from - 22 to - 10‰ (Degens et al., 1968; Sackett et al., 1965; Sharp, 2006).

The Orcau dataset shows rather low values of $\delta^{13}C_{carb}$, falling coincidentally with $\delta^{18}O$ throughout the Upper Aren Unit (Fig. 3); this could mark the input of fresh water with the more proximal facies found at the top of the succession. The isotopic record would suggest more and more terrestrial (meteoric water) input. In the Aren Fm deltaic deposits, the preserved OM is probably mainly terrestrial with the presence of continental vitrinite and inertinite (Figs. 7, 8) and probably pollen and spores coming from the continent, together with

491 quartzitic and lithic grains as are often found in deltaic successions (Martinez et al., 2002;
492 Stukins et al., 2013). The high sedimentation flux and erosive characteristics explains the
493 difficulty in finding both a large number of foraminifera and well-preserved microfossils in
494 samples. Thus the marine OM, such as planktonic oceanic components and algal debris,
495 probably represents a small proportion of the oceanic OM, except in some part of the Upper
496 Aren Unit. At higher resolution the four sequences of the Upper Aren Unit (CuS1 to CuS4)
497 show generally more negative $\delta^{13}C_{carb}$ values towards the top of the sedimentary shallowing-
498 up sequences (Fig. 11), supporting the idea that $\delta^{13}C_{carb}$ values are driven partly by the
499 increase of meteoric water in the deltaic environment. Simultaneously the $\delta^{13}C_{org}$ increases
500 upwards in CuS1 and CuS2, is very chaotic in CuS3, and decreases in CuS4 (Fig. 11). The
501 CuS1 and particularly the CuS2 signal may indicate an increase of terrestrial input
502 throughout the coarsening-up sequences. Conversely, the negative trend of the CuS4 could
503 indicate an increase in photic organisms despite the regressive sedimentary signal. However
504 rudist patches are reported laterally indicating sheltered areas probably well adapted for
505 some photic blooms the OM of which may be incorporated into the deltaic system. The
506 chaotic signal of CuS3 together with the very thick and high-hydrodynamical deltaic
507 sandstones could indicate a mix of OM from marine and terrestrial input.

508 At the boundary between the Aren Fm and the Grey Unit, the sharp shift in the geochemical
509 proxies could suggest an unconformity (Fig. 11). However this sharp shift corresponds to an
510 abrupt paleoenvironmental and lithological change (marine to lagoonal environments) that
511 may induce a change from stable conditions towards more complex interaction and variability
512 among salinity, energy, and trophic conditions, mimicking an unconformity. The Grey Unit
513 basal deposits show the most negative $\delta^{13}C_{org}$ values (- 27,15‰) while the marl and
514 sandstone deposits of the Grey Unit show the most positive isotopic values. The latter might
515 correspond to a mix of light terrestrial OM and some OM from photic organisms such as
516 ostracods. Less terrestrial debris trapped in the lagoonal marshes, and more photic
517 contributions (mainly from charophytes and ostracods) could be driving the $\delta^{13}C_{org}$ values

towards less negative values. Moreover it is clear that the Grey Unit displays a variety of salinities well observed in skeletal carbonates (Oms et al, 2016) that might produce geochemically complex signals.

The very negative $\delta^{13}C_{carb}$ values in the top part of the succession (Grey Unit) are linked with high TOC content and a positive swing in the $\delta^{18}O$. The negative values of $^{13}C_{carb}$ could be driven by burial diagenesis of the organic-rich claystone beds. Indeed sulfate-reduction processes occur during the burial of organic claystone, leading to remineralization of the OM and authigenic carbonate precipitation depleted in ^{13}C (Bodin et al., 2016; Wohlwend et al., 2016). Lighter O (variation of 4‰ in the $\delta^{18}O$) in the Grey Unit could suggest an impact of less saline water in the lagoonal environment on the recorded isotopic fractionation, the meteoric water driving the O values towards more positive values.

4.3 $\delta^{13}C_{carb}$ and $\delta^{13}C_{org}$ signal comparison

At a geological time scale, it is accepted that various reservoirs are likely to record $\delta^{13}C$ fluctuations simultaneously (Koch et al., 1992), and C transfer can be considered as instantaneous. So when disturbances in the carbon cycle occur they are recorded in both marine and continental sediments (e.g. Gröcke, 1998; Hasegawa et al., 2003; Jahren et al., 2001; Magioncalda et al., 2001; Tsikos et al., 2004). It is therefore possible to compare both marine and terrestrial isotopic signals (e.g. Magioncalda et al., 2004) either in mineral carbon ($\delta^{13}C_{carb}$) or in organic carbon ($\delta^{13}C_{org}$).

Some studies have shown that the $\delta^{13}C$ record of marine organic matter can be correlated with the $\delta^{13}C$ of organic matter of lagoonal environments, but from terrestrial origin (Heimhofer et al., 2003). In addition, several studies comparing $\delta^{13}C_{org}$ and $\delta^{13}C_{carb}$ performed on the same section show simultaneous trends in both signals, with different absolute values (Magioncalda et al., 2001; Storme et al., 2014; Tsikos et al., 2004).

Our dataset tends to confirm that both signals record comparable sequences (S1 to S11; Fig. 9) in the full succession, with similar boundaries. However, the $\delta^{13}C_{carb}$ and $\delta^{13}C_{org}$ signals

often show inverse trends (S2, S3, S5, S6; Fig. 11). For example, the interval interpreted as the LCE shows an opposing variation in the signal values. The Grey Unit presents a very noticeable shift in all geochemical proxies as this unit presents a relatively high TOC content and a positive shift of $\delta^{18}O$ towards lighter values, while the $\delta^{13}C_{carb}$ and $\delta^{13}C_{org}$ show very distinctive values, part of this may be due to OM remineralization as discussed previously (Figs. 3, 11).

Value variations in $\delta^{13}C_{org}$ show a larger spectrum and the signal is not easy to compare. It is a challenging proxy to use, therefore, particularly in a context of mixed OM and water origin (e.g. terrestrial and marine). Overall the $\delta^{13}C_{org}$ variations record changes relatively simultaneously to global events recorded in the $\delta^{13}C_{carb}$ dataset (Fig. 11), which corroborates previous work that has demonstrated that the $\delta^{13}C_{org}$ primary signal reflects the composition of the environmental CO_2 available at that time (Kump and Arthur, 1999). It should be a good record of global geochemical events when coupled with other proxies.

The biological environment is partly responsible for the variations in the isotopic record, however (Dunkley Jones et al., 2010). It seems clear that sedimentary dynamics are also accountable for some variations. Indeed, while geochemical sequences do not coincide with sedimentary sequences in the deepest-water environment (in the lower Upper Aren Unit), changes in geochemical records follow sedimentary sequences in the deltaic system (Fig. 11). Thus the deciphering of global geochemical records must be carried out at the same time as the understanding of local parameters. Particularly one must be very careful when interpreting the origin of $\delta^{13}C_{org}$ trends because the variations may be due to changes both in the OM types and origin, that make the use of this proxy much more complex.

Conclusion

The very thick Campano-Maastrichtian deltaic succession of the Tremp-Graus Basin contains rare and poorly preserved biostratigraphic markers despite the rudist-patch and lagoonal facies that provide some biostratigraphic markers. The magnetic signals allow some

570 chron determinations (Fondevilla et al., 2016; Oms et al., 2007, 2016), in particular the
571 definition of the boundary between C32 and C31r (Maastrichtian) at the boundary between
572 the Upper Aren Unit and the base of the Grey Unit. More biostratigraphical constraints were
573 found with the presence of *Siderolites* with well-developed spines (sample OR-02-21)
574 indicating that this bed (at 198 m) is Maastrichtian in age, but these are insufficient for a
575 more precise stratigraphical framework. Hence, we provided a continuous $\delta^{13}C_{carb}$, $\delta^{13}C_{org}$
576 and $\delta^{18}O$ dataset for the 325 meter-thick Orcau succession, encompassing various facies
577 from deltaic to lagoonal environments, making it the first attempt at a multiproxy isotopic
578 analysis of Upper Cretaceous detrital (shoreface) deposits. The carbon isotope excursions
579 and trends of the $\delta^{13}C$ dataset allow the determination of some global geochemical events
580 when comparing them to the reference sections of Gubbio and Tercis-les-Basin, and
581 enabling global climatic events such as the CMBE to be identified. The LCE is also strongly
582 suspected to be present at the base of the section. The isotopic record of the Orcau section
583 shows a C_{carb} signal that can be related to global changes, while the shift to lower values in
584 the uppermost parts of the Aren Fm can be linked to palaeo-environmental drivers such as
585 more meteoric input (less saline water in a deltaic setting closer to shore). In the Grey Unit,
586 however, the very low values are probably related to claystone burial effects and an OM-rich
587 succession that induced OM remineralization and the authigenetic production of carbonate
588 with lighter C. Nevertheless in this Grey Unit the higher values in the $\delta^{18}O$ may record a
589 palaeo-environmental effect of poorly saline lagoonal water.

590 The studied succession in the Tremp-Graus Basin is complex due to various coeval
591 palaeoenvironmental factors, such as high-energy deltaic environments of the Aren Fm and
592 lateral rudist patches. Changes in palaeo-environments, OM inputs and lithology might have
593 an impact on isotopic values, and particularly on the $\delta^{13}C_{org}$. The origin of the analyzed OM
594 and its role in the variation of signal is to be questioned (e.g. Maufrangeas et al., 2020) for
595 two reasons: (1) in fluvio-deltaic sediments such as the Aren Fm marine and continental OM
596 were mixed in unknown proportion, both types bearing different fractionation values; and (2)

597 in detrital sediments, it is possible some OM is reworked. Despite this complexity, it can be
598 assumed that (1) the proportion of continental vs marine OM does not change throughout the
599 deltaic studied succession, and that the terrestrial OM might be dominant, and (2) that the
600 reworked OM is in minute proportion and diluted in the sample. Working on the bulk C_{org} and
601 therefore on the mean (continental and marine) $\delta^{13}C_{org}$ makes it possible to minimize the
602 biological effects. Some excursions or trends in the $\delta^{13}C_{org}$ signal can be related to global
603 changes as the shifts are coeval, despite some decorrelated/ inverse responses. They are
604 better observed in the deepest environments (lower part of the study succession), but in the
605 uppermost deltaic sequences, the $\delta^{13}C_{org}$ signal cannot be interpreted, probably due to many
606 erosional surfaces that truncate the records. When dividing the signal of the $\delta^{13}C_{carb}$ and
607 $\delta^{13}C_{org}$ in geochemical sequences, the boundaries for which are defined when the signal
608 changes, it is noteworthy that they coincide with the deltaic sequences in the Upper Aren
609 Unit. Part of the signal is thus clearly driven by local palaeo-environmental changes, but the
610 overall global signal can be detected nevertheless.

611 The $\delta^{13}C$ is a useful method to improve the stratigraphy in shoreface deposits, but one must
612 be particularly cautious in the interpretation of the geochemical excursions and trends
613 because of the presence of sedimentary hiatuses and potential variations of the signal.
614 Particularly in the C_{org} proxy, changes in the types and dominant sources of organic matter
615 might induce changes in the $\delta^{13}C_{org}$ signal, unrelated to atmospheric variations. The
616 magnetostratigraphic coherence, the rare biostratigraphic markers, and the pattern of the
617 CIE isotope data, permits global indicators to be interpreted in the Orcau succession, despite
618 its location in a deltaic environment.

619 **Acknowledgements**

620 This study is part of a PhD project funded by the Orogen Project (Total/BRGM/CNRS). We
621 are grateful to Brigitte Spiterri at the University of Bordeaux Montaigne and Alexandra Coynel
622 at the University of Bordeaux who made available to us their crusher for sample lab

623 preparation. We are grateful to Thomas Rigaudier for his help in the geochemistry lab of the
624 CRPG lab in Nancy (University of Lorraine) for the TOC and $\delta^{13}C_{org}$ measurements. We wish
625 to thanks B. Bennani and S. Yameogo for sampling and grinding most samples, and S. Fetati
626 for picking the foraminifera. Thanks to Philippe Razin for his support and discussions
627 regarding the geology of the Pyrenees, and Dr Liam Herringshaw for a final English
628 correction. We address special acknowledgments to one anonymous reviewer, Oriol Oms
629 and editor Eduardo Koutsoukos for their thorough comments leading to the improvement of
630 initial manuscript.

631 **Reference**

632 Ardèvol, L., Klimowitz, J., Malagón, J., and Nagtegaal, P. J. C., 2000. Depositional Sequence
633 Response to Foreland Deformation in the Upper Cretaceous of the Southern Pyrenees,
634 Spain. *AAPG Bulletin* 84 (4): 566-87. https://doi.org/10.1306/C9EBCE55-1735-11D7-
635 8645000102C1865D.
636 Arens, N. C., and Jahren A. H., 2000. Carbon Isotope Excursion in Atmospheric CO2 at the
637 Cretaceous-Tertiary Boundary: Evidence from Terrestrial Sediments. *Palaios* 15 (4):
638 314-22. https://doi.org/10.1669/0883-1351(2000)015<0314:CIEIAC>2.0.CO;2.
639 Arens, N. C., Jahren, A. H., and Amundson, R., 2000. Can C3 Plants Faithfully Record the
640 Carbon Isotopic Composition of Atmospheric Carbon Dioxide? *Paleobiology* 26 (1):
641 137-64. https://doi.org/10.1666/0094-8373(2000)026<0137:CCPFRT>2.0.CO;2.
642 Arz, J. A., and Molina, E., 2002. Late Campanian and Maastrichtian biostratigraphy and
643 chronostratigraphy based on planktic foraminifera in temperate and subtropical
644 latitudes (Spain, France and Tunisia). *N. Jb. Geol. Palaont. Abh. 224*, 2002.
645 Aubry, M-P., Khaled, O., Dupuis, C., Berggren, W. A., Van Couvering, J.A., Ali, J., Brinkhuis,
646 H., et al., 2007. The Global Standard Stratotype-section and Point (GSSP) for the base
647 of the Eocene Series in the Dababiya section. https://doi.org/10.7916/D8BP0C85.

Bodin, S., Mau, M., Sadki, D., Danisch, J., Nutz, A., Krencher, F-N., Kabiri, L., 2020. Transient and secular changes in global carbon cycling during the early Bajocian event: Evidence for Jurassic cool climate episodes. *Global and Planetary Change* 194. https://doi.org/10.1016/j.gloplacha.2020.103287

Bodin, S., Krencker, F. N., Kothe, T., Hoffmann, R., Mattioli, E., Heimhofer, U., and Kabiri, L., 2016. Perturbation of the carbon cycle during the late Pliensbachian–early Toarcian: New insight from high-resolution carbon isotope records in Morocco. *Journal of African Earth Sciences*, *116*, 89-104.

Canudo, J.I., Oms, O., Vila, B., Galobart, À., Fondevilla, V., Puértolas-Pascual, E., Sellés, A.G., Cruzado-Caballero, P., Dinarès-Turell, J., Vicens, E., Castanera, D., Company, J., Burrel, L., Estrada, R., Marmi, J., Blanco, A., 2016. The upper Maastrichtian dinosaur fossil record from the southern Pyrenees and its contribution to the topic of the Cretaceous– Palaeogene mass extinction event. *Cretaceous Research* 57: 540–551. http://dx.doi. org/10.1016/j.cretres.2015.06.013.

Caus, E., Frijia, G., Parente, M., Robles-Salcedo, R., and Villalonga, R., 2016. Constraining the Age of the Last Marine Sediments in the Late Cretaceous of Central South Pyrenees (NE Spain): Insights from Larger Benthic Foraminifera and Strontium Isotope Stratigraphy. *Cretaceous Research* 57 : 402‑413. https://doi.org/10.1016/j.cretres.2015.05.012.

Caus, E., and Gómez-Garrido, A., 1989. Upper cretaceous biostratigraphy of the south-central Pyrenees (Lleida, Spain). *Geodinamica Acta* 3 (3): 221‑28. https://doi.org/10.1080/09853111.1989.11105188.

Cerling, T.E., and Quade, J., 1993. Stable Carbon and Oxygen Isotopes in Soil Carbonates. In *Geophysical Monograph Series*, P. K. Swart, K. C. Lohmann, J. Mckenzie, and S. Savin, (eds) 217‑31. Washington, D. C.: American Geophysical Union. https://doi.org/10.1029/GM078p0217.

674 Chenot, E., Pellenard, P., Martinez, M., Deconinck, J. F., Amiotte-Suchet, P., Thibault, N., ...
675 & Robaszynski, F., 2016. Clay mineralogical and geochemical expressions of the “Late
676 Campanian Event” in the Aquitaine and Paris basins (France): Palaeoenvironmental
677 implications. *Palaeogeography, Palaeoclimatology, Palaeoecology*, *447*, 42-52.
678 Coccioni, R., Bancalà, G., Catanzarit, R., Fornaciari, E., Frontalini, F., Giusberti, L., Jovane,
679 L., Luciani V., Savian, J., and Sprovieri, M., 2012. An integrated stratigraphic record of
680 the Palaeocene–lower Eocene at Gubbio (Italy): new insights into the early Palaeogene
681 hyperthermals and carbon isotope excursions. *Terra Nova* 24 (5): 380-86.
682 https://doi.org/10.1111/j.1365-3121.2012.01076.x.
683 Cojan, I., Moreau, M.-G., and Stott, L. E., 2000. Stable Carbon Isotope Stratigraphy of the
684 Paleogene Pedogenic Series of Southern France as a Basis for Continental-Marine
685 Correlation. *Geology* 28 (3): 259-62. https://doi.org/10.1130/0091-
686 7613(2000)28<259:SCISOT>2.0.CO;2.
687 Cojan, I., Renard, M., and Emmanuel, L., 2003. Palaeoenvironmental reconstruction of
688 dinosaur nesting sites based on a geochemical approach to eggshells and associated
689 palaeosols (Maastrichtian, Provence Basin, France). *Palaeogeography,*
690 *Palaeoclimatology, Palaeoecology* 191 (2): 111-38. https://doi.org/10.1016/S0031-
691 0182(02)00655-7.
692 Cuevas, J.L., 1992. Estratigrafia del “Garimniense” de la Conca de Tremp. Prepirineo de
693 Lérida . *Acta Geologica Hispanica* 27.
694 Cuevas, J.L., Dreyer, T., and Mercade, L., 1989. The first stage of the foreland basin: the
695 Tremp Group. In *Guidebook 4th Int. Conference on Fluvial Sedimentology*, Muñoz A.,
696 (eds.u).
697 Deramond, J., Souquet, P., Fondecave-Wallez, M—J., Specht, M., 1993. Relationships
698 between thrust tectonics and sequence stratigraphy surfaces in foredeeps: model and
699 examples from the Pyrenees (Cretaceous-Eocene, France, Spain). In WILLIAMS, G. D.

& DOBB, A. (eds). *Tectonics and Seismic Sequence Stratigraphy*. Geological Society Special Publication 71: 193-219. https://doi.org/10.1144/GSL.SP.1993.071.01.09

Degens, E. T., Guillard, R. R. L., Sackett, W. M., & Hellebust, J. A., 1968. Metabolic fractionation of carbon isotopes in marine plankton—I. Temperature and respiration experiments. In *Deep Sea Research and Oceanographic Abstracts*, 15(1), 1-9. Elsevier.

Díaz-Molina, M., 1987. Sedimentación sinectónica asociada a una subida relativa del nivel del mar durante el Cretácico superior (Fm. Tremp, provincia de Lérida). *Estudios Geológicos* 43 (Extra): 69-93. https://doi.org/10.3989/egeol.8743Extra626.

Díez-Canseco, D., Arz, J. A., Benito, M. I., Díaz-Molina, M., and Arenillas, I., 2014. Tidal influence in redbeds: A palaeoenvironmental and biochronostratigraphic reconstruction of the Lower Tremp Formation (South-Central Pyrenees, Spain) around the Cretaceous/Paleogene boundary. *Sedimentary Geology* 312 (octobre): 31-49. https://doi.org/10.1016/j.sedgeo.2014.06.008.

Dunkley, J., T., Ridgwell, A., Lunt, D. J., Maslin, M. A., Schmidt, D. N., and Valdes, P. J., 2010. A Palaeogene Perspective on Climate Sensitivity and Methane Hydrate Instability. *Philosophical Transactions of the Royal Society A: Mathematical, Physical and Engineering Sciences* 368 (1919): 2395-2415. https://doi.org/10.1098/rsta.2010.0053.

Feist, M., and Colombo, Piñol F., 1983. La limite Crétacé-Tertiaire dans le nord-est de l'Espagne, du point de vue des charophytes. *Géologie Méditerranéenne* 10 (3): 303-25. https://doi.org/10.3406/geolm.1983.1273.

Föllmi, K. B., Godet, A., Bodin, S., and Linder, P., 2006. Interactions between Environmental Change and Shallow Water Carbonate Buildup along the Northern Tethyan Margin and Their Impact on the Early Cretaceous Carbon Isotope Record. *Paleoceanography* 21 (4). https://doi.org/10.1029/2006PA001313.

726 Fondevilla, V., Dinarès-Turell, J., and Oms, O., 2016. The Chronostratigraphic Framework of
727 the South-Pyrenean Maastrichtian Succession Reappraised: Implications for Basin
728 Development and End-Cretaceous Dinosaur Faunal Turnover. *Sedimentary Geology*
729 337 (mai): 55‑68. https://doi.org/10.1016/j.sedgeo.2016.03.006.
730 Gale, A. S., Jenkyns, H. C., Kennedy, W. J., and Corfield, R. M., 1993. Chemostratigraphy
731 versus Biostratigraphy: Data from around the Cenomanian–Turonian Boundary.
732 *Journal of the Geological Society* 150 (1): 29‑32.
733 https://doi.org/10.1144/gsjgs.150.1.0029.
734 Gröcke, D.R., 1998. Carbon-Isotope Analyses of Fossil Plants as a Chemostratigraphic and
735 Palaeoenvironmental Tool. *Lethaia* 31 (1): 1‑13. https://doi.org/10.1111/j.1502-
736 3931.1998.tb00482.x.
737 Hasegawa, T., Pratt, L.M., Maeda, H., Shigeta, Y., Okamoto, T., Kase, T., and Uemura, K.,
738 2003. Upper Cretaceous Stable Carbon Isotope Stratigraphy of Terrestrial Organic
739 Matter from Sakhalin, Russian Far East: A Proxy for the Isotopic Composition of
740 Paleoatmospheric CO2. *Palaeogeography, Palaeoclimatology, Palaeoecology* 189 (1-
741 2): 97‑115. https://doi.org/10.1016/S0031-0182(02)00634-X.
742 Hayes, J. M, Popp, B. N., Takigiku, R., and Johnson, M. W., 1989. An isotopic study of
743 biogeochemical relationships between carbonates and organic carbon in the
744 Greenhorn Formation. *Geochimica et Cosmochimica Acta* 53 (11): 2961‑72.
745 https://doi.org/10.1016/0016-7037(89)90172-5.
746 Heimhofer, U., Hochuli, P. A., Burla, S., Andersen, N., and Weissert, H., 2003. Terrestrial
747 Carbon-Isotope Records from Coastal Deposits (Algarve, Portugal): A Tool for
748 Chemostratigraphic Correlation on an Intrabasinal and Global Scale. *Terra Nova* 15
749 (1): 8‑13. https://doi.org/10.1046/j.1365-3121.2003.00447.x.
750 Hilting, A. K., Kump, L. R., & Bralower, T. J., 2008. Variations in the oceanic vertical carbon
751 isotope gradient and their implications for the Paleocene-Eocene biological pump.
752 *Paleoceanography*, *23*(3).

753 Hoyt, J.H., 1967. Occurrence of high-angle stratification in littoral and shallow nericitc
754 environments, Central Georgia Coast, U.S.A. *Sedimentology* 8: 229-238.
755 https://doi.org/10.1111/j.1365-3091.1967.tb01322.x

756 Jahren, A. H., Amundson, R., Kendall, C., and Wigand, P., 2001. Paleoclimatic
757 Reconstruction Using the Correlation in δ ^{18} O of Hackberry Carbonate and
758 Environmental Water, North America. *Quaternary Research* 56 (2): 252-63.
759 https://doi.org/10.1006/qres.2001.2259.

760 Jarvis, I., Gale, A.S., Jenkyns, H. C., and Pearce, M.A., 2006. Secular Variation in Late
761 Cretaceous Carbon Isotopes: A New Δ13C Carbonate Reference Curve for the
762 Cenomanian–Campanian (99.6–70.6 Ma). *Geological Magazine* 143 (5): 561-608.
763 https://doi.org/10.1017/S0016756806002421.

764 Jarvis, I., Mabrouk, A., Moody, R. T. J, and de Cabrera, S., 2002. Late Cretaceous
765 (Campanian) carbon isotope events, sea-level change and correlation of the Tethyan
766 and Boreal realms. *Palaeogeography, Palaeoclimatology, Palaeoecology* 188 (3): 215-
767 48. https://doi.org/10.1016/S0031-0182(02)00578-3.

768 Jenkyns, H. C., Gale, A. S., and Corfield, R. M., 1994. Carbon- and Oxygen-Isotope
769 Stratigraphy of the English Chalk and Italian Scaglia and Its Palaeoclimatic
770 Significance. *Geological Magazine* 131 (1): 1-34.
771 https://doi.org/10.1017/S0016756800010451.

772 Jung, C., Voigt, S., and Friedrich, O., 2012. High-resolution carbon-isotope stratigraphy
773 across the Campanian–Maastrichtian boundary at Shatsky Rise (tropical Pacific).
774 *Cretaceous Research* 37: 177-85. https://doi.org/10.1016/j.cretres.2012.03.015.

775 Khozyem, H., Adatte, T., Spangenberg, J.E., Tantawy, A.A., and Keller, G., 2013.
776 Palaeoenvironmental and Climatic Changes during the Palaeocene–Eocene Thermal
777 Maximum (PETM) at the Wadi Nukhul Section, Sinai, Egypt. *Journal of the Geological*
778 *Society* 170 (2): 341-52. https://doi.org/10.1144/jgs2012-046.

779 Koch, P.L., Zachos, J.C., and Gingerich, P.D., 1992. Correlation between Isotope Records in
780 Marine and Continental Carbon Reservoirs near the Palaeocene/Eocene Boundary.
781 *Nature* 358 (6384): 319. https://doi.org/10.1038/358319a0.
782 Kump, L.R., and Arthur, M.A., 1999. Interpreting carbon-isotope excursions: carbonates and
783 organic matter. *Chemical Geology* 161 (1): 181‑98. https://doi.org/10.1016/S0009-
784 2541(99)00086-8.
785 Linnert, C., Robinson, A, Lees, S. A., Pérez-Rodríguez, J., Jenkyns I.C, Petrizzo H.R.M., ... &
786 Falzoni, F., 2017. Did Late Cretaceous cooling trigger the Campanian–Maastrichtian
787 Boundary Event?. *Newsletters on Stratigraphy*. http://doi.org/10.1127/nos/2017/0310
788 Lopez, S., Cojan, I., and Renard, M., 2000. Corrélations chimiostratigraphiques entre
789 domaines marin et continental : application à une série du Miocène inférieur (Beynes-
790 Châteauredon, Alpes-de-Haute-Provence, France). *Comptes Rendus de l'Académie*
791 *des Sciences - Series IIA - Earth and Planetary Science* 330 (12): 837‑43.
792 https://doi.org/10.1016/S1251-8050(00)00224-X.
793 López Martínez, N., Arribas Mocoroa, M. E., Robador, A., Vicens, E., & Ardèvol, L., 2006.
794 Los carbonatos danienses (Unidad 3) de la Fm Tremp (Pirineos sur-centrales):
795 paleogeografía y relación con el límite Cretácico-Terciario. *Revista de la Sociedad*
796 *Geológica de España*, *19*(3-4), 233-255.
797 López-Martínez, N., Canudo, J.I., Ardèvol, L., Pereda Suberbiola, X., Orue-Etxebarria, X.,
798 Cuenca-Bescós, G., Ruiz-Omeñaca, J.I., Murelaga, X., and Feist, M., 2001. New
799 dinosaur sites correlated with Upper Maastrichtian pelagic deposits in the Spanish
800 Pyrenees: implications for the dinosaur extinction pattern in Europe. *Cretaceous*
801 *Research* 22 (1): 41‑61. https://doi.org/10.1006/cres.2000.0236.
802 Magioncalda, R., Dupuis, C., Blamart, D., Fairon-Demaret, M., Perreau, M., Renard, M.,
803 Riveline, J., Roche, M., and Keppens, E., 2001. L'excursion Isotopique Du Carbone
804 Organique (Delta 13 C Org) Dans Les Paleoenvironnements Continentaux de

l'intervalle Paleocene/Eocene de Varangeville (Haute-Normandie). *Bulletin de La Société Géologique de France* 172 (3): 349–58. https://doi.org/10.2113/172.3.349.

Magioncalda, R., Dupuis, C., Smith, T., Steurbaut, E., and Gingerich, P. D., 2004. Paleocene-Eocene Carbon Isotope Excursion in Organic Carbon and Pedogenic Carbonate: Direct Comparison in a Continental Stratigraphic Section. *Geology* 32 (7): 553–56. https://doi.org/10.1130/G20476.1.

Martinez, M. A., Quattrocchio, M. E., and Zavala, C. A., 2002. Analisis palinofacial de la formacion Lajas (Jurasico medio), uenca neuquina, Argentina. Significado paleoambiental y paleoclimatico. *Revista española de micropaleontología*, 2002.

Maufrangeas, A., Leleu, S., Loisy, C., Roperch, P., Jolley, D., Vinciguerra, C., and Nguyen-Thuyet, O., 2020. Stratigraphy in Palaeocene Continental Sedimentary Succession of the Northern Pyrenean Basin (Corbières, Southern France) Using $\delta^{13} C_{org}$ Isotopes. *Journal of the Geological Society*. https://doi.org/10.1144/jgs2019-084.

McInerney, F.A., and Wing, S. L., 2011. The Paleocene-Eocene Thermal Maximum: A Perturbation of Carbon Cycle, Climate, and Biosphere with Implications for the Future. *Annual Review of Earth and Planetary Sciences* 39 (1): 489–516. https://doi.org/10.1146/annurev-earth-040610-133431.

Mey, P. H. W., Nagtegaal, P. J. C., Roberti, K. J., and Hartevelt, J. J. A., 1968. Lithostratigraphic Subdivision of Post-Hercynian Deposits in the South-Central Pyrenees, Spain. *Leidse Geologische Mededelingen* 41 (1): 221–28.

Muñoz, J. A., 1992. Evolution of a Continental Collision Belt: ECORS-Pyrenees Crustal Balanced Cross-Section. In *Thrust Tectonics*, K. R. McClay (ed), 235–46. Dordrecht: Springer Netherlands. https://doi.org/10.1007/978-94-011-3066-0_21.

Mutti, E, and Sgavetti, M., 1987. Sequence stratigraphy of the Upper Cretaceous Aren strata in the Aren–Orcau region, south-central Pyrenees, Spain: Distinction between eustatically and tectonically controlled depositional sequences. *Annali dell'Universita´ di Ferrara* 1*:* 1–22.

832 Nagtegaal, P. J. C., Van Vliet A., and Brouwer, J., 1983. Syntectonic coastal offlap and
833 concurrent turbidite deposition: The Upper Cretaceous Aren sandstone in the South-
834 Central Pyrenees, Spain. *Sedimentary Geology* 34 (2): 185-218.
835 https://doi.org/10.1016/0037-0738(83)90086-6.
836 Nagtegaal, P.J.C., 1972. Depositional history and clay minerals of the Upper Cretaceous
837 basin in the South-Central Pyrenees, Spain. *Leidse Geologische Mededelingen* 47 (2):
838 251-75.
839 Oehlert, A. and Swart, P., 2014. Interpreting carbonate and organic carbon isotope
840 covariance in the sedimentary record. *Nature communications* 5: 4672.
841 10.1038/ncomms5672.
842 Ogg, J.G., and Hinnov, L.A., 2012. Cretaceous. *In:* Gradstein, F. M., Ogg, J. G., Schmitz, M.
843 B., & Ogg, G. M. (Eds.). *The geologic time scale 2012*, Elsevier, Amsterdam, 793-853.
844 Oms, O., Dinarès-Turell, J., Vicens, E., Estrada, R., Vila, B., Galobart, À., and Bravo, A.M.,
845 2007. Integrated Stratigraphy from the Vallcebre Basin (Southeastern Pyrenees,
846 Spain): New Insights on the Continental Cretaceous–Tertiary Transition in Southwest
847 Europe. *Palaeogeography, Palaeoclimatology, Palaeoecology* 255 (1-2): 35-47.
848 https://doi.org/10.1016/j.palaeo.2007.02.039.
849 Oms, O., Fondevilla, V., Riera, V., Marmi, J., Vicens, E., Estrada, R., Anadón, P., Vila, B.,
850 and Galobart, À., 2016. Transitional Environments of the Lower Maastrichtian South-
851 Pyrenean Basin (Catalonia, Spain): The Fumanya Member Tidal Flat. *Cretaceous*
852 *Research* 57: 428-42. https://doi.org/10.1016/j.cretres.2015.09.004.
853 Paul, C.R.C., and Lamolda, M. A., 2007. Carbon and Oxygen Stable Isotopes in the
854 Maastrichtian of the Basque Country, N. Spain. *Cretaceous Research* 28 (5): 812-20.
855 https://doi.org/10.1016/j.cretres.2006.12.003.
856 Pereda-Suberbiola, X., Canudo, J.I., Cruzado-Caballero, P., Barco, J.L., López-Martínez, N.,
857 Oms, O., and Ruiz-Omeñaca, J.I., 2009. The last hadrosaurid dinosaurs of Europe: A

858 new lambeosaurine from the Uppermost Cretaceous of Aren (Huesca, Spain).
859 *Comptes Rendus Palevol* 8 : 559-572. https://doi.org/10.1016/j.crpv.2009.05.002

860 Petrizzo, M. R., 2001. Late Cretaceous Planktonic Foraminifera from Kerguelen Plateau
861 (ODP Leg 183): New Data to Improve the Southern Ocean Biozonation. *Cretaceous*
862 *Research* 22 (6): 829-55. https://doi.org/10.1006/cres.2001.0290.

863 Puigdefàbregas, C., Muñoz, J. A., and Vergés, J., 1992. Thrusting and Foreland Basin
864 Evolution in the Southern Pyrenees. In *Thrust Tectonics*, K. R. McClay (ed), 247-54.
865 Dordrecht: Springer Netherlands. http://link.springer.com/10.1007/978-94-011-3066-
866 0_22.

867 Puigdefàbregas, C., and Souquet, P., 1986. Tecto-sedimentary cycles and depositional
868 sequences of the Mesozoic and Tertiary from the Pyrenees. *Tectonophysics* 129 (1):
869 173-203. https://doi.org/10.1016/0040-1951(86)90251-9.

870 Pujalte, V., and Schmitz, B., 2005. Revisión de la estratigrafía del Grupo Tremp
871 («Garumniense», Cuenca de Tremp-Graus, Pirineos meridionales), Geogaceta 38: 79-
872 82. http://rabida.uhu.es/dspace/handle/10272/8757.

873 Riera, V., Marmi, J., Oms, O., and Gomez, B., 2010. Orientated plant fragments revealing
874 tidal palaeocurrents in the Fumanya mudflat (Maastrichtian, southern Pyrenees):
875 Insights in palaeogeographic reconstructions. *Palaeogeography, Palaeoclimatology,*
876 *Palaeoecology* 288 (1): 82-92. https://doi.org/10.1016/j.palaeo.2010.01.037.

877 Riera, V., Oms, O., Gaete, R., and Galobart, À., 2009. The End-Cretaceous Dinosaur
878 Succession in Europe: The Tremp Basin Record (Spain). *Palaeogeography,*
879 *Palaeoclimatology, Palaeoecology* 283 (3-4): 160-71.
880 https://doi.org/10.1016/j.palaeo.2009.09.018.

881 Riera, V., Anadón, P., Oms, O., Estrada, R., and Maestro, E., 2013. Dinosaur eggshell
882 isotope geochemistry as tools of palaeoenvironmental reconstruction for the
883 upper Cretaceous from the Tremp Formation (Southern Pyrenees). *Sedimentary*
884 *Geology* 294: 356-370. https://doi.org/10.1016/j.sedgeo.2013.06.001

885 Robles-Salcedo, R., 2014. Family Siderolitidae (Upper Cretaceous larger foraminifera):
886 architecture, biostratigraphy, paleoenvironimental distributionand paleobiogeography.
887 Robles-Salcedo, R., Vicedo, V., and Caus, E., 2018. Latest Campanian and Maastrichtian
888 Siderolitidae (Larger Benthic Foraminifera) from the Pyrenees (S France and NE
889 Spain). *Cretaceous Research* 81: 64-85. https://doi.org/10.1016/j.cretres.2017.08.017.
890 Robles-Salcedo, R., Rivas, G., Vicedo, V., and Caus, E., 2013. Paleoenvironmental
891 distribution of larger foraminifera in upper cretaceous siliciclastic–carbonate deposits
892 (arén sandstone formation, south pyrenees, northeastern spain). *Palaios* 28 (9): 637-
893 48. https://doi.org/10.2110/palo.2012.p12-125r.
894 Röhl, U., Westerhold, T., Bralower, T. J., and Zachos, J.C., 2007. On the Duration of the
895 Paleocene-Eocene Thermal Maximum (PETM): PALEOCENE-EOCENE THERMAL
896 MAXIMUM. *Geochemistry, Geophysics, Geosystems* 8 (12): n/a-n/a.
897 https://doi.org/10.1029/2007GC001784.
898 Rosell, J., Linares, R., and Llompart, C., 2001. EL “GARUMNIENSE” PREPIRENAICO.
899 Sackett, W. M., Eckelmann, W. R., Bender, M. L., and Bé, A. W. 1965. Temperature
900 dependence of carbon isotope composition in marine plankton and sediments.
901 *Science 148*(3667): 235-237.
902 Sharp, Z.D., 2006. Principles of stable isotope geochemistry, Pearson, 2nd edition, 360p.
903 Sheldon, E., Ineson, J., and Bown, P., 2010. Late Maastrichtian warming in the Boreal
904 Realm: Calcareous nannofossil evidence from Denmark. *Palaeogeography,*
905 *Palaeoclimatology, Palaeoecology* 295 (1): 55-75.
906 https://doi.org/10.1016/j.palaeo.2010.05.016.
907 Souquet, P., 1967. Le Crétacé supérieur Sud-Pyrénéen en Catalogne, Aragon et Navarre.
908 Souquet, P., and Deramond, J., 1989. Séquence de chevauchements et séquences de dépôt
909 dans un bassin d’avant-fosse. Exemple du sillon crétacé du versant sud des Pyrénées
910 (Espagne). *Séquence de chevauchements et séquences de dépôt dans un bassin*

911 *d'avant-fosse. Exemple du sillon crétacé du versant sud des Pyrénées (Espagne)* 309
912 (1): 137‑44.
913 Storme, J-Y., Devleeschouwer, X., Schnyder, J., Cambier, G., Baceta, J. I., Pujalte, V., Di
914 Matteo, A., Iacumin, P., and Yans, J., 2012. The Palaeocene/Eocene Boundary
915 Section at Zumaia (Basque-Cantabric Basin) Revisited: New Insights from High-
916 Resolution Magnetic Susceptibility and Carbon Isotope Chemostratigraphy on Organic
917 Matter (Δ13Corg). *Terra Nova* 24 (4): 310‑17. https://doi.org/10.1111/j.1365-
918 3121.2012.01064.x.
919 Storme, J-Y., Steurbaut, E., Devleeschouwer, X., Dupuis, C., Iacumin, P., Rochez, G., and
920 Yans, J., 2014. Integrated bio-chemostratigraphical correlations and climatic evolution
921 across the Danian–Selandian boundary at low latitudes. *Palaeogeography,*
922 *Palaeoclimatology, Palaeoecology* 414: 212‑24.
923 https://doi.org/10.1016/j.palaeo.2014.09.002.
924 Storme, J-Y., 2013. Organic Carbon and Nitrogen Isotopes of the Palaeocene-early Eocene:
925 Implcations on Stratigraphy, Paleoenvironment and Paleoclimatology. PhD.
926 Stukins, S., Jolley, D.W., McIlroy, D., and Hartley, A.J., 2013. Middle Jurassic Vegetation
927 Dynamics from Allochthonous Palynological Assemblages: An Example from a
928 Marginal Marine Depositional Setting; Lajas Formation, Neuquén Basin, Argentina.
929 *Palaeogeography, Palaeoclimatology, Palaeoecology* 392 (décembre): 117‑27.
930 https://doi.org/10.1016/j.palaeo.2013.09.002.
931 Teixell, A. and Muñoz,J.A., 2000. Evolucion tectoni-sedimentaria del Pirineo merdional
932 durante el Terciario: una sintesis basada en la transversal del rio Noguera Ribagoçana.
933 *Rev. Soc. Geol. Espaiia, 13 (2)*, 2000.
934 Thibault, N., Harlou, R., Schovsbo, N., Schiøler, P., Minoletti, F., Galbrun, B., Lauridsen,
935 B.W., Sheldon, E., Stemmerik, L., and Surlyk, F., 2012. Upper Campanian–
936 Maastrichtian nannofossil biostratigraphy and high-resolution carbon-isotope
937 stratigraphy of the Danish Basin: Towards a standard δ13C curve for the Boreal

Realm. *Cretaceous Research* 33 (1): 72-90. https://doi.org/10.1016/j.cretres.2011.09.001.

Tsikos, H., Jenkyns, H. C., Walsworth-Bell, B., Petrizzo, M. R., Forster, A., Kolonic, S., Erba, E., 2004. Carbon-Isotope Stratigraphy Recorded by the Cenomanian–Turonian Oceanic Anoxic Event: Correlation and Implications Based on Three Key Localities. *Journal of the Geological Society* 161 (4): 711-19. https://doi.org/10.1144/0016-764903-077.

Vacherat, A., Mouthereau, F., Pik, R., Huyghe, D., Paquette, J. L., Christophoul, F., ... & Tibari, B., 2017. Rift-to-collision sediment routing in the Pyrenees: A synthesis from sedimentological, geochronological and kinematic constraints. *Earth-Science Reviews*, *172*, 43-74.

Vergés, J., Fernàndez, M., and Martìnez, A., 2002. The Pyrenean Orogen: Pre-, Syn-, and Post-Collisional Evolution. *Journal of the Virtual Explorer* 08. https://doi.org/10.3809/jvirtex.2002.00058.

Vicens, E., Ardèvol, L., Lopès-Martinez, N., and Arribas, M. E., 2004. Rudist Biostratigraphy in the Campanian – Maastrichtian of the south-central Pyrenees, Spain. *Cour. Forsch.-Inst. Senckenberg, 247*, 2004.

Vicente, A., Martín-Closas, C., Arz, J.A., and Oms, O., 2015. Maastrichtian-basal Paleocene charophyte biozonation and its calibration to the Global Polarity Time Scale in the southern Pyrenees (Catalonia, Spain). *Cretaceous Research* 52: 268-285. https://doi.org/10.1016/j.cretres.2014.10.004.

Villalba-Breva, S., and Martín-Closas, C., 2012. Upper Cretaceous Paleogeography of the Central Southern Pyrenean Basins (Catalonia, Spain) from Microfacies Analysis and Charophyte Biostratigraphy. *Facies* 59 (2): 319-45. https://doi.org/10.1007/s10347-012-0317-1.

Voigt, S., Friedrich, O., Norris, R. D., and Schönfeld, J., 2010. Campanian – Maastrichtian Carbon Isotope Stratigraphy: Shelf-Ocean Correlation between the European Shelf

965 Sea and the Tropical Pacific Ocean. *Newsletters on Stratigraphy* 44 (1): 57‑72.
966 https://doi.org/10.1127/0078-0421/2010/0004.
967 Voigt, S., Gale, A.S., Jung, C., and Jenkyns, H.C., 2012. Global Correlation of Upper
968 Campanian – Maastrichtian Successions Using Carbon-Isotope Stratigraphy:
969 Development of a New Maastrichtian Timescale. *Newsletters on Stratigraphy* 45 (1): 25
970 ‑53. https://doi.org/10.1127/0078-0421/2012/0016.
971 Wendler, I., 2013. A critical evaluation of carbon isotope stratigraphy and biostratigraphic
972 implications for Late Cretaceous global correlation. *Earth-Science Reviews* 126
973 (novembre): 116‑46. https://doi.org/10.1016/j.earscirev.2013.08.003.
974 Westerhold, T., Röhl, U., Donner, B., McCarren, H.K., and Zachos, J.C., 2011. A Complete
975 High-Resolution Paleocene Benthic Stable Isotope Record for the Central Pacific (ODP
976 Site 1209): PALEOCENE BENTHIC STABLE ISOTOPE RECORD. *Paleoceanography*
977 26 (2): n/a-n/a. https://doi.org/10.1029/2010PA002092.
978 Wohlwend, S., Hart, M., & Weissert, H., 2016. Chemostratigraphy of the Upper Albian to mid-
979 Turonian Natih Formation (Oman) – how authigenic carbonate changes a global
980 pattern. *The Depositional Record*, *2*(1), 97-117.
981 Yans, J., Marandat, B., Masure, E., Serra-Kiel, J., Schnyder, J., Storme, J-Y., Marivaux, L.,
982 Adnet, S., Vianey-Liaud, M., and Tabuce, R., 2014. Refined Bio- (Benthic Foraminifera,
983 Dinoflagellate Cysts) and Chemostratigraphy ($\delta\,^{13}C_{org}$) of the Earliest Eocene at Albas-
984 Le Clot (Corbières, France): Implications for Mammalian Biochronology in Southern
985 Europe . *Newsletters on Stratigraphy* 47 (3): 331‑53.
986 https://doi.org/10.1127/nos/2014/0050.
987

988 **Captions**

989 Figure 1: Geological setting for the study section: (A) Tremp-Graus Basin geological map; (B)
990 Location of the Campanian – Maastrichtian sedimentary and geochemical sections (1) this

991 study: the Orcau section in the Tremp-Graus Basin (Spain), (2) Tercis-les-Bains reference
992 section in the French Basque Country (Voigt et al., 2012), and (3) Gubbio reference section
993 in Italy (Voigt et al., 2012; Coccioni et al., 2012); (C) Stratigraphy of the Tremp-Graus Basin

994 Figure 2: The study Orcau Log section showing facies variability, specific sedimentary
995 structures and sequences. Depositional environments are indicated as well as
996 lithostratigraphic and stratigraphic assignment which was better constrained with the
997 magnetostratigraphic chrons from Fondevilla et al. (2016). The polygon shows the
998 Campanian – Maastrichtian boundary from previous studies and the star highlights the
999 updated boundary from this study. Samples are located along the log for biostratigraphical
1000 analysis and red diamond for the organic matter (OM) petrographic analysis. Distribution of
1001 planktonic foraminifera, benthic foraminifera and other bioclasts observed are indicated for
1002 residues (black dots) and for thin sections (white dots).

1003 Figure 3: Geochemical results along the Orcau section: isotope analysis ($\delta^{13}C_{org}$, $\delta^{13}C_{carb}$,
1004 $\delta^{18}O$), TOC (%), and $CaCO_3$ (%).The polygon shows the Campanian – Maastrichtian
1005 boundary from previous studies and the star highlights the updated boundary from this study.

1006 Figure 4: Scanning electron micrograph illustrations of planktonic foraminifera from the Orcau
1007 Section: 1a-c. *Globotruncana mariei* (OR03-86); 2a-c. *Globotruncana arca* (0R-03-76); 3a-c.
1008 *Globotruncana hilli* (OR17); 4a-c. *Globotruncana linneiana* (OR09); 5a-c. *Rugotruncana*
1009 *subcircumnodifer* (OR17); 6a-c. *Globotruncana aegyptiaca* (OR17); 7a-c. *Contusotruncana*
1010 *morozovae* (OR09); 8a-c. *Muricohedbergella holmdelensis* (OR19); 9a-b. *Planoheterohelix*
1011 *globulosa* (OR19); 10a-b. *Planoheterohelix labellosa* (OR17); 11a-c. *Rugoglobigerina rugosa*
1012 (OR-03-86); 12a-b. *Globigerinelloides prairiehillensis* (OR19); 13a-b. *Globigerinelloides*
1013 *messinae* (OR19). Scale bar : 200 μm.

1014 Figure 5: Detailed microfacies (thin sections) of the Orcau Section (Upper Aren Unit). A. OR-
1015 02-23, Marine microfacies with orbitoids; B.OR-02-08, Bioclastics microfacies with bryozoan;
1016 C., D., E. OR-02-21, Marine microfacies with diverse benthic organisms (C. Textulariina,

Miliolina (*Fallotia*) orbitoids and red algae, D. orbitoids and *Siderolites*, E. *Siderolites* with well-developed spines); F. OR-02-26, Lagoonal microfacies with charophytes; G., H. OR-03-297, Lagoonal microfacies with charophytes, gasterods and ostracods. Scale bar : 1 mm.

Figure 6: Key benthic and planktonic foraminifera. Maastrichtian *Siderolites* with well-developed spines (thin section, Upper Aren Unit, OR-03-214). Scale bar : 1 mm.

Figure 7: Organic matter petrographic analysis in optical microscopy, 50x objective, reflexion light in oil immersion; (A) observation in natural light (OR03-158) and (B) same section, in fluorescent light, in which amorphous marine OM can be detected; (C) observation in natural light (OR03-158) and (D) same section in fluorescent light; observations in natural light of continental vitrinite (E) in OR03-191 and (F) in OR03-158; observations of continental telinite (G) in OR03-158 and (H) in OR03-191.

Figure 8: Organic matter petrographic analysis in optical microscopy, 50x objective, reflexion light in oil immersion; observations of OR03-158 in natural light (A) rounded grain of continental vitrinite, (B) and (C) angular debris of continental vitrinite and (D) gelified particule of OM; and observations in fluorescent light of mixt non florescent continental OM and marine florescent amorphous OM in OR03-191 (E), and OR03-158 (F) and (G), and of continental leptinite in OR03-191 (H).

Figure 9: Cross-plots of (a) $\delta^{13}C_{carb}$ *vs* $\delta^{18}O$, (b) $\delta^{13}C_{org}$ *vs* $\delta^{13}C_{carb}$, (c) $\delta^{13}C_{carb}$ *vs* TOC, (d) $\delta^{13}C_{org}$ *vs* TOC. In the crossplots linear regressions and R_2-values were calculated for the each stratigraphic unit that represents samples deposited under very different environments i.e. the Lower Aren Unit, the Upper Aren Unit and the Grey Unit.

Figure 10: Correlation scheme in the Campanian-Maastrichtian interval of the (1) Orcau dataset, (2) Tercis-les-Bains reference section; dataset from Voigt et al., 2012 and (3) Gubbio reference section; dataset from Voigt et al., 2012; Coccioni et al., 2012: carbon isotope dataset (this work), biostratigraphic constrains (this work) and magnetostratigraphy polarity chrons (Fondevilla et al., 2016) correlated with the two reference marine sections

1043 calibrated with high-resolution biostratigraphy and magnetostratigraphy across the
1044 Campanian to Maastrichtian times, where the global geochemical events were defined
1045 and/or well recognized.

1046 Figure 11: Comparison of the $\delta^{13}C_{org}$ and $\delta^{13}C_{carb}$ signal and TOC content in the study Orcau
1047 section.

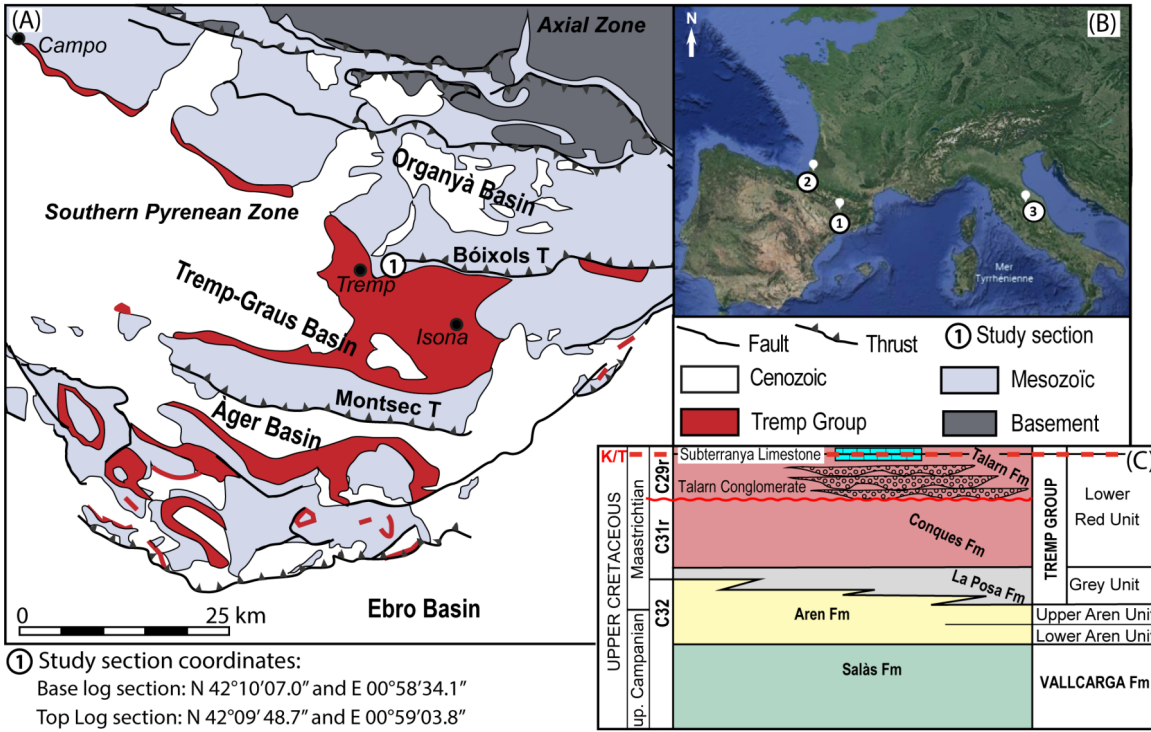

① Study section coordinates:

Base log section: N 42°10′07.0″ and E 00°58′34.1″

Top Log section: N 42°09′ 48.7″ and E 00°59′03.8″

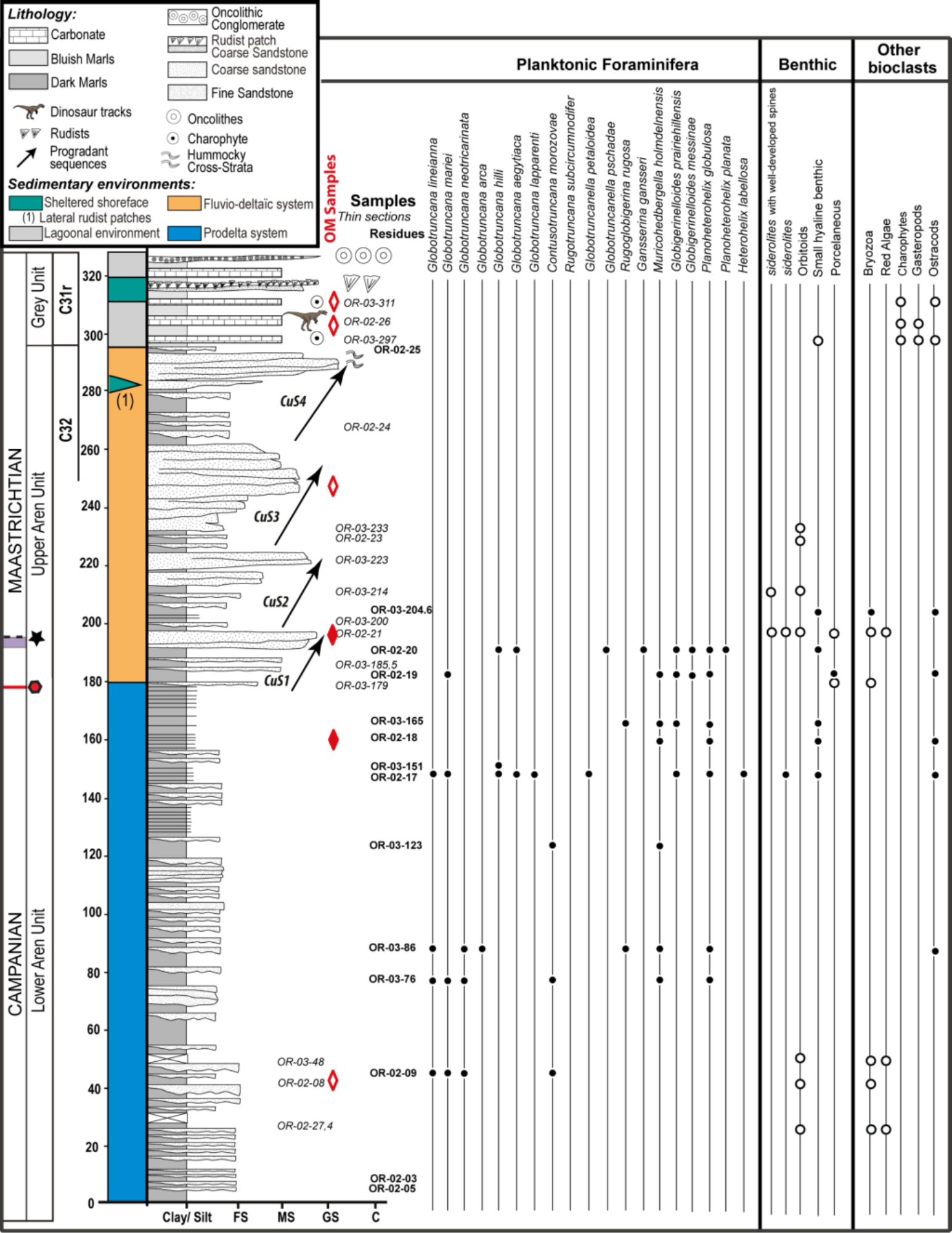
Lithology:
Carbonate
Bluish Marls
Dark Marls
Dinosaur tracks
Rudists
Progradant sequences
Oncolithic Conglomerate
Rudist patch Coarse Sandstone
Coarse sandstone
Fine Sandstone
Oncolithes
Charophyte
Hummocky Cross-Strata
Sedimentary environments:
Sheltered shoreface
(1) Lateral rudist patches
Lagoonal environment
Fluvio-deltaïc system
Prodelta system
Planktonic Foraminifera
Benthic
Other bioclasts
Samples
Thin sections
Residues
OM Samples
Globotruncana lineianna
Globotruncana mariei
Globotruncana neotricarinata
Globotruncana arca
Globotruncana hilli
Globotruncana aegytiaca
Globotruncana lapparenti
Contusotruncana morozovae
Rugotruncana subcircumnodifer
Globotruncanella petaloidea
Globotruncanella pschadae
Rugoglobigerina rugosa
Gansserina gansseri
Muricohedbergella holmdelnensis
Globigerinelloides prairiehillensis
Globigerinelloides messinae
Planoheterohelix globulosa
Planoheterohelix planata
Heterohelix labellosa
siderolites with well-developed spines
siderolites
Orbitoids
Small hyaline benthic
Porcelaneous
Bryozoa
Red Algae
Charophytes
Gasteropods
Ostracods
MAASTRICHTIAN
CAMPANIAN
Grey Unit
Upper Aren Unit
Lower Aren Unit
C31r
C32
(1)
CuS4
CuS3
CuS2
CuS1
OR-03-311
OR-02-26
OR-03-297
OR-02-25
OR-02-24
OR-03-233
OR-02-23
OR-03-223
OR-03-214
OR-03-204.6
OR-03-200
OR-02-21
OR-02-20
OR-03-185,5
OR-02-19
OR-03-179
OR-03-165
OR-02-18
OR-03-151
OR-02-17
OR-03-123
OR-03-86
OR-03-76
OR-03-48
OR-02-09
OR-02-08
OR-02-27,4
OR-02-03
OR-02-05
320
300
280
260
240
220
200
180
160
140
120
100
80
60
40
20
0
Clay/ Silt
FS
MS
GS
C

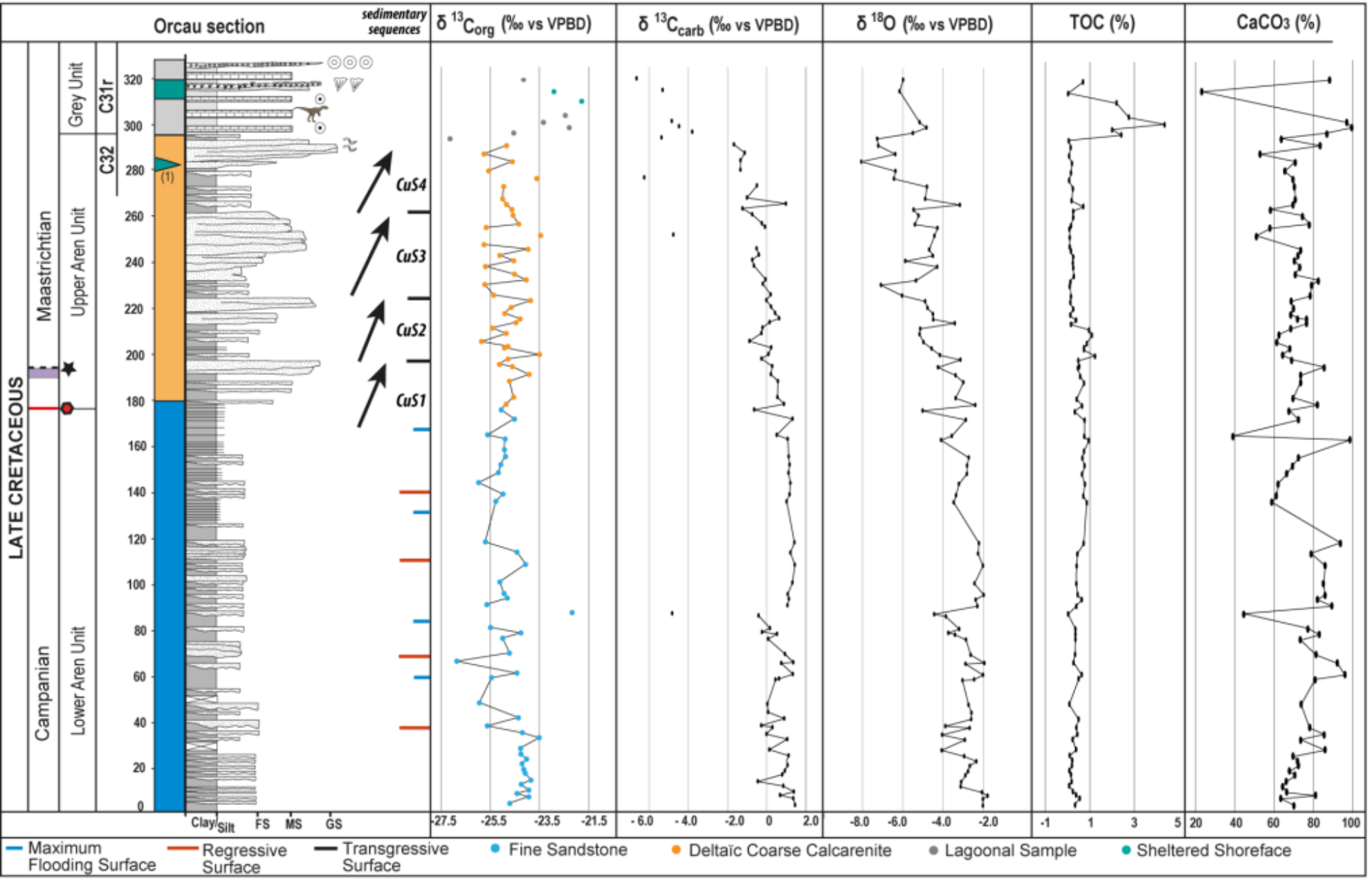
Orcau section
sedimentary sequences
δ 13Corg (‰ vs VPBD)
δ 13Ccarb (‰ vs VPBD)
δ 18O (‰ vs VPBD)
TOC (%)
CaCO3 (%)
LATE CRETACEOUS
Maastrichtian
Campanian
Grey Unit
Upper Aren Unit
Lower Aren Unit
C31r
C32
(1)
CuS4
CuS3
CuS2
CuS1
Clay
Silt
FS
MS
GS
-27.5
-25.5
-23.5
-21.5
- 6.0
- 4.0
-2.0
0
2.0
-8.0
-6.0
-4.0
-2.0
-1
1
3
5
20
40
60
80
100
Maximum Flooding Surface
Regressive Surface
Transgressive Surface
Fine Sandstone
Deltaïc Coarse Calcarenite
Lagoonal Sample
Sheltered Shoreface

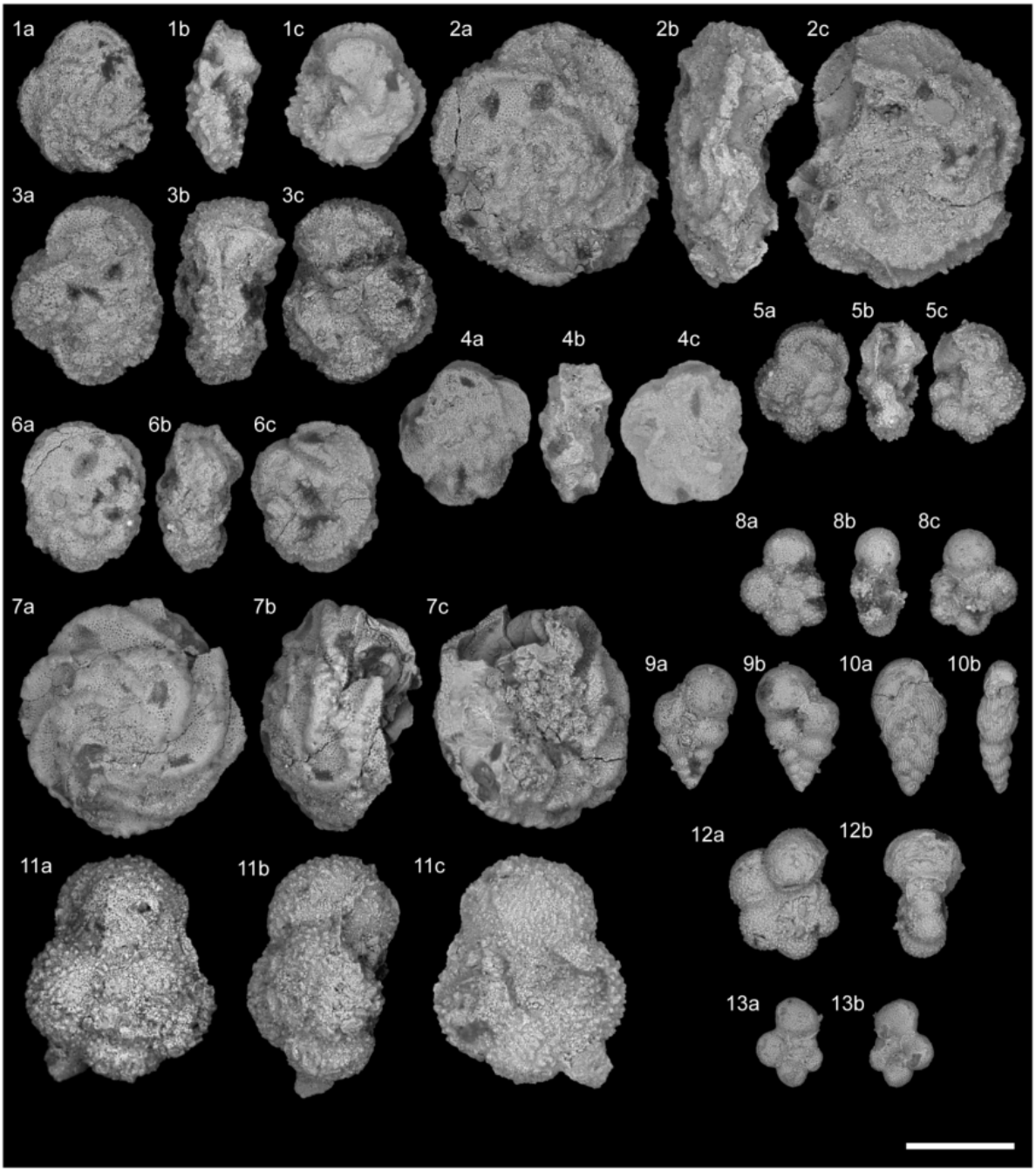
1a
1b
1c
2a
2b
2c
3a
3b
3c
4a
4b
4c
5a
5b
5c
6a
6b
6c
7a
7b
7c
8a
8b
8c
9a
9b
10a
10b
11a
11b
11c
12a
12b
13a
13b

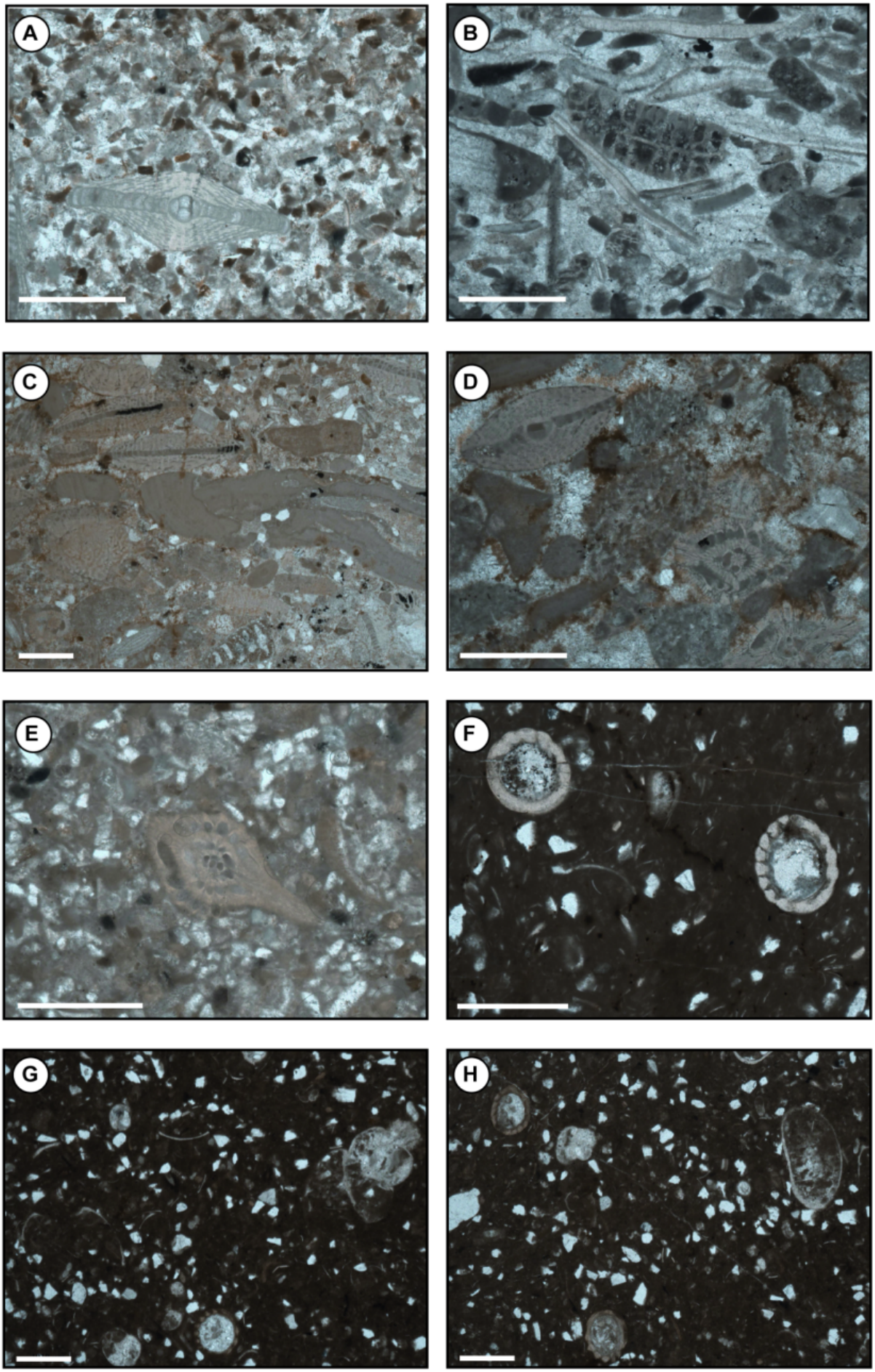
A
B
C
D
E
F
G
H

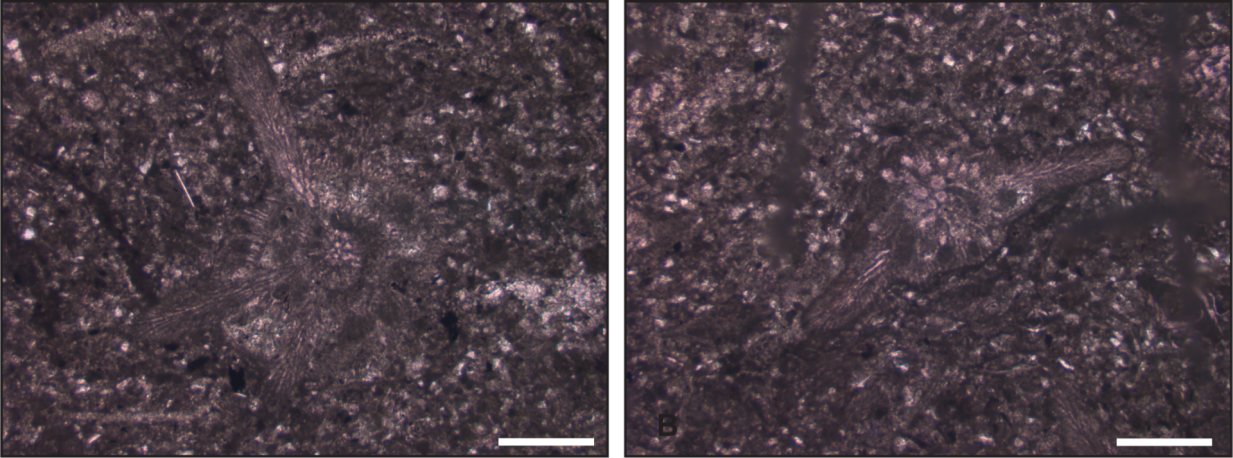
B

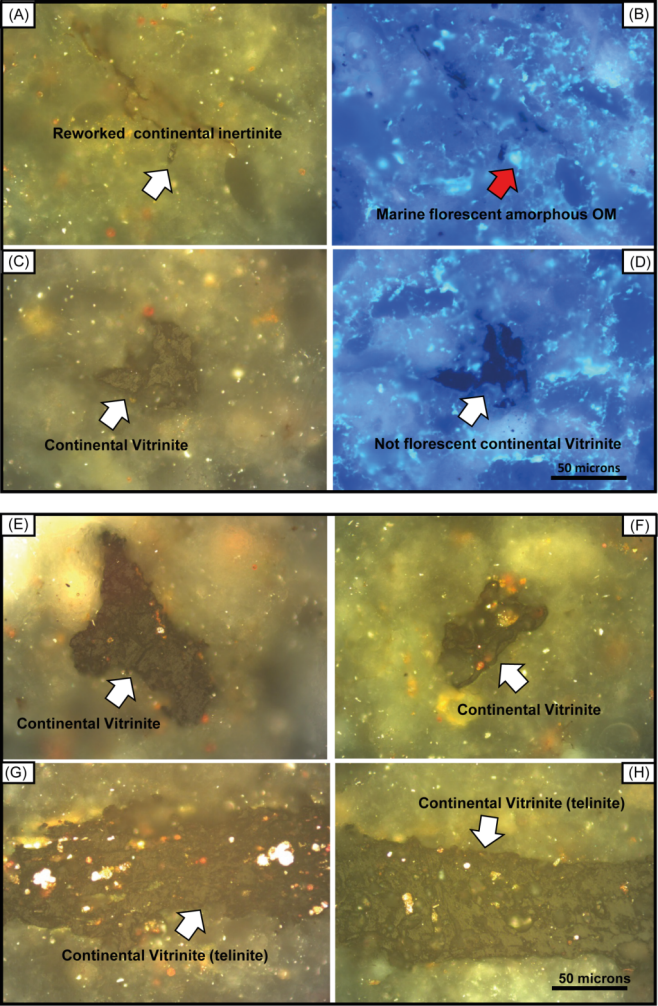
(A)
Reworked continental inertinite
(B)
Marine florescent amorphous OM
(C)
Continental Vitrinite
(D)
Not florescent continental Vitrinite
50 microns
(E)
Continental Vitrinite
(F)
Continental Vitrinite
(G)
Continental Vitrinite (telinite)
(H)
Continental Vitrinite (telinite)
50 microns

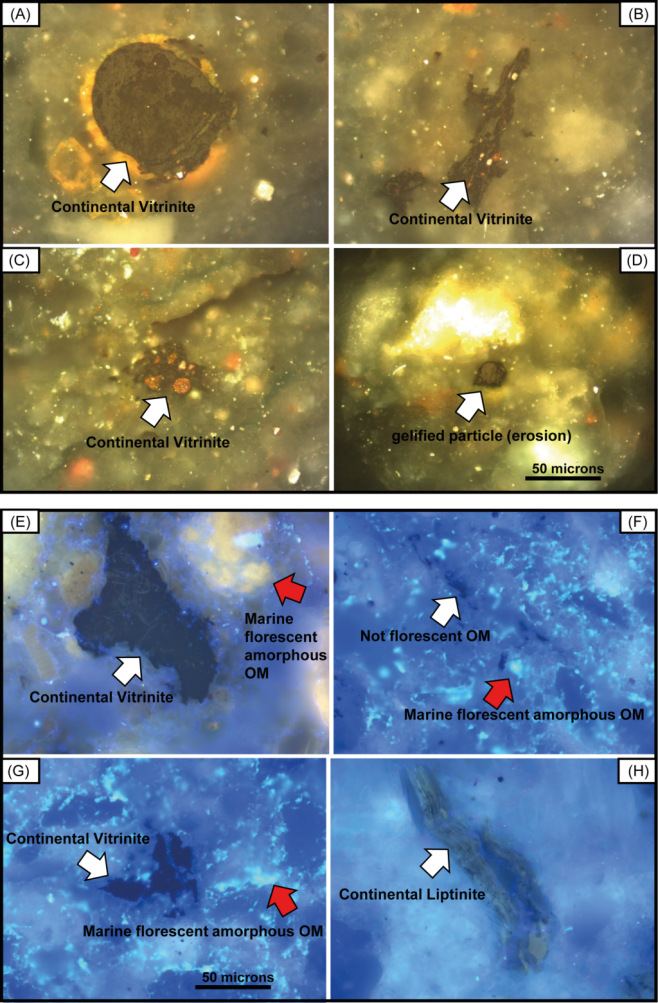
(A)
Continental Vitrinite
(B)
Continental Vitrinite
(C)
Continental Vitrinite
(D)
gelified particle (erosion)
50 microns
(E)
Marine florescent amorphous OM
Continental Vitrinite
(F)
Not florescent OM
Marine florescent amorphous OM
(G)
Continental Vitrinite
Marine florescent amorphous OM
50 microns
(H)
Continental Liptinite

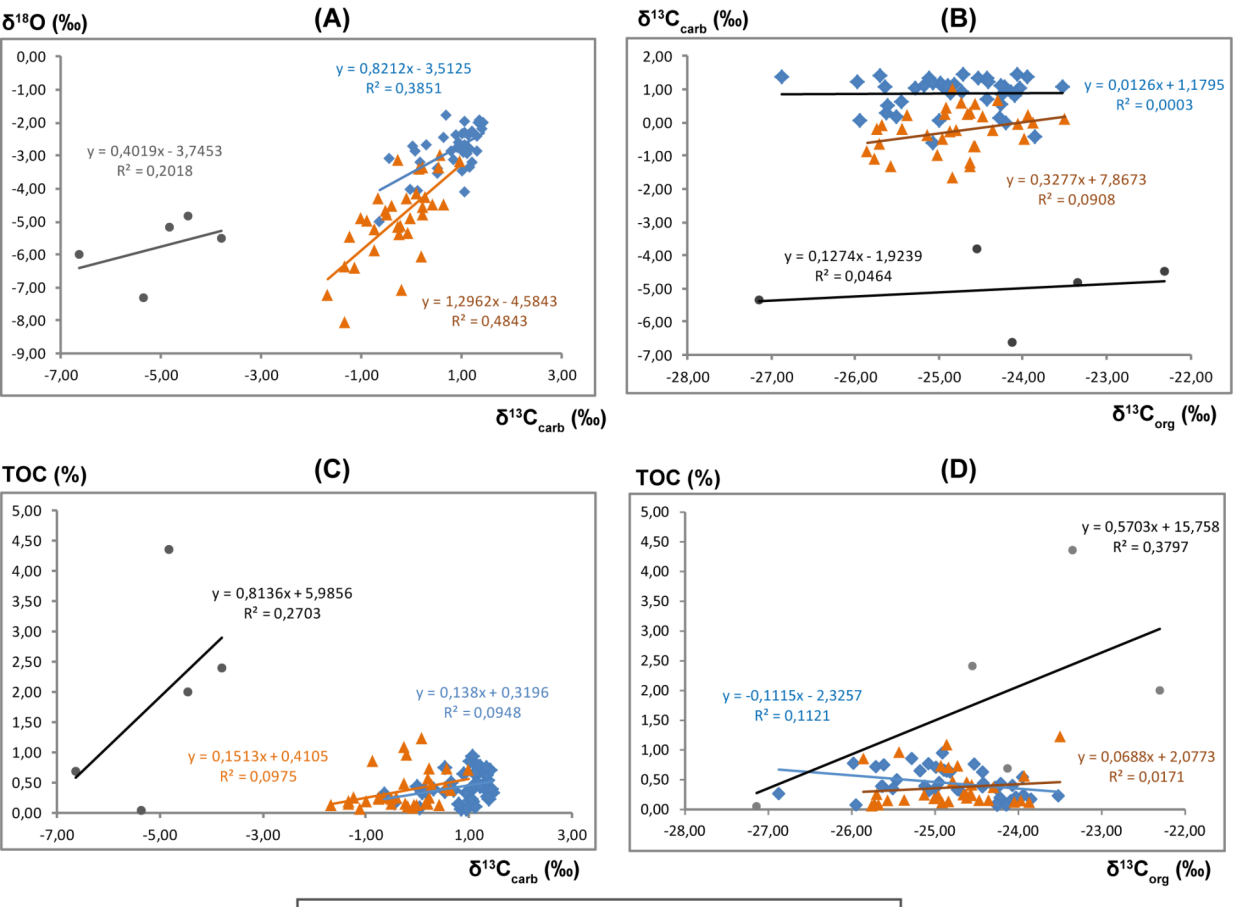
δ18O (‰)
(A)
y = 0,8212x - 3,5125
R² = 0,3851
y = 0,4019x - 3,7453
R² = 0,2018
y = 1,2962x - 4,5843
R² = 0,4843
δ13Ccarb (‰)
δ13Ccarb (‰)
(B)
y = 0,0126x + 1,1795
R² = 0,0003
y = 0,3277x + 7,8673
R² = 0,0908
y = 0,1274x - 1,9239
R² = 0,0464
δ13Corg (‰)
TOC (%)
(C)
y = 0,8136x + 5,9856
R² = 0,2703
y = 0,138x + 0,3196
R² = 0,0948
y = 0,1513x + 0,4105
R² = 0,0975
δ13Ccarb (‰)
TOC (%)
(D)
y = 0,5703x + 15,758
R² = 0,3797
y = -0,1115x - 2,3257
R² = 0,1121
y = 0,0688x + 2,0773
R² = 0,0171
δ13Corg (‰)
Lower Aren Unit
Upper Aren Unit
Grey Unit

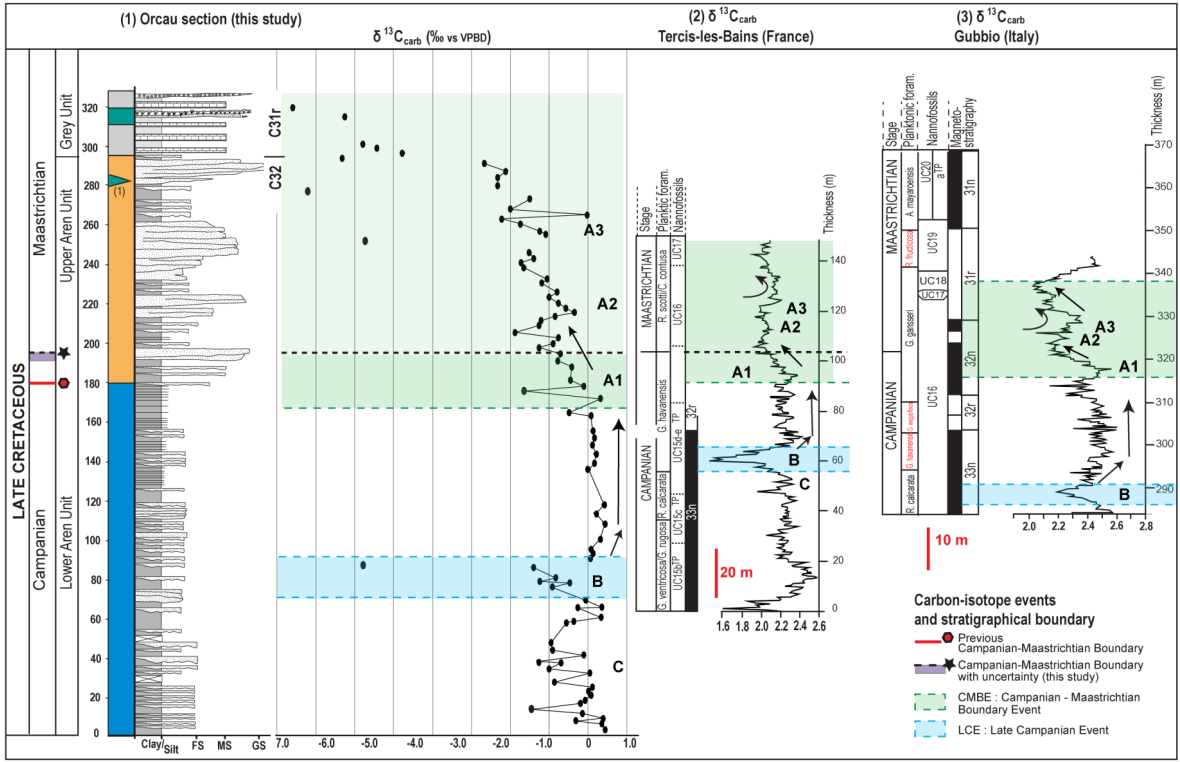
(1) Orcau section (this study)
δ 13Ccarb (‰ vs VPBD)
(2) δ 13Ccarb
Tercis-les-Bains (France)
(3) δ 13Ccarb
Gubbio (Italy)
LATE CRETACEOUS
Maastrichtian
Campanian
Upper Aren Unit
Lower Aren Unit
Grey Unit
Clay
Silt
FS
MS
GS
C31r
C32
A1
A2
A3
B
C
Stage
Planktonic foram.
Nannofossils
Magneto-stratigraphy
Thickness (m)
MAASTRICHTIAN
CAMPANIAN
R. scotticus
A. mayaroensis
G. gansseri
G. havanensis
R. calcarata
G. ventricosa/G. rugosa
UC20
UC19
UC18
UC17
UC16
UC15e
UC15c
UC15b
31n
31r
32n
32r
33n
20 m
10 m
Carbon-isotope events
and stratigraphical boundary
Previous
Campanian-Maastrichtian Boundary
Campanian-Maastrichtian Boundary
with uncertainty (this study)
CMBE : Campanian - Maastrichtian
Boundary Event
LCE : Late Campanian Event

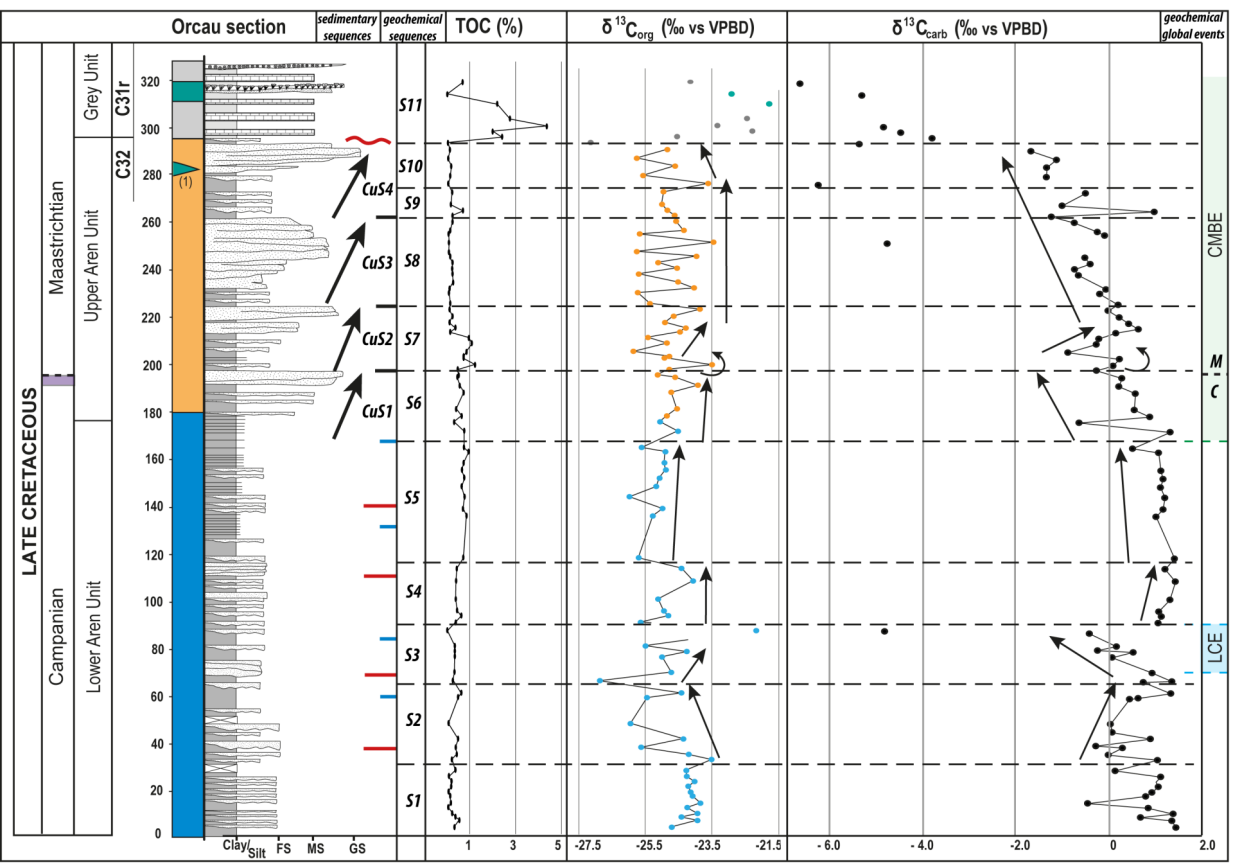
Orcau section
sedimentary sequences
geochemical sequences
TOC (%)
δ13Corg (‰ vs VPBD)
δ13Ccarb (‰ vs VPBD)
geochemical global events
LATE CRETACEOUS
Campanian
Maastrichtian
Lower Aren Unit
Upper Aren Unit
Grey Unit
C31r
C32
(1)
CuS4
CuS3
CuS2
CuS1
S11
S10
S9
S8
S7
S6
S5
S4
S3
S2
S1
CMBE
MIC
LCE
Clay/Silt
FS
MS
GS